Research Square

Preprints are preliminary reports that have not undergone peer review.
They should not be considered conclusive, used to inform clinical practice,
or referenced by the media as validated information.

Underwater explosive forming of thin metallic plates using repeated blast loading: improving die filling while controlling thinning

Mohammad Kouzehgaran
Imam Hossein University
Hossein Khodarahmi
Imam Hossein University
Milad Sadegh-Yazdi
msadeghy@ihu.ac.ir

Imam Hossein University
Mojtaba Ziya-Shamami
Imam Hossein University
Tohid Mirzababaie Mostofi
University of Eyvanekey

Research Article

Keywords: Underwater explosive forming, Female die–forming, Repeated blast loading, Coupled Eulerian–Lagrangian approach, High strain–rate forming

Posted Date: July 1st, 2026

DOI: https://doi.org/10.21203/rs.3.rs-10038506/v1

License: This work is licensed under a Creative Commons Attribution 4.0 International License.
Read Full License

Additional Declarations: No competing interests reported.

Version of Record: A version of this preprint was published at International Journal of Material Forming on September 11th, 2026. See the published version at https://doi.org/10.1007/s12289-026-02080-0.

Underwater explosive forming of thin metallic plates using repeated blast loading: improving die filling while controlling thinning

Mohammad Kouzehgaran [a], Hossein Khodarahmi [a], Milad Sadegh-Yazdi*[a], Mojtaba Ziya-Shamami [a], Tohid Mirzababaie Mostofi [b]

[a] Department of Mechanical Engineering, Faculty of Engineering, Imam Hossein University, Tehran, Iran

[b] Department of Mechanical Engineering, University of Eyvanekey, Eyvanekey, Iran

Abstract

Explosive forming offers a flexible route for shaping metallic sheets into dies, but a single explosion at room temperature can limit formability and die filling. This study experimentally and numerically investigates underwater forming of a 3 mm thick plate into a female die using repeated blast loading. Metallic specimens were subjected to single, double, and triple explosions, and the outcomes were assessed in terms of sheet thinning and die-filling percentage. In single-shot forming, increasing the charge mass beyond 5 g caused reverse deflection in the central region, led to a maximum thinning of 36.7%, and still failed to achieve full die filling (81.4%). In contrast, the use of second and third underwater blasts enabled complete die filling with reduced thinning and a lower total explosive charge. A coupled Eulerian–Lagrangian (CEL) model in ABAQUS/Explicit was employed to examine deformation velocity, Von Mises stress (SMises), equivalent plastic strain (PEEQ), and the Johnson–Cook damage initiation parameter (JCCRT). Double-explosion tests showed higher SMises, PEEQ, and JCCRT, while no red (damaged) zones appeared on either face of specimens formed with triple explosions. Using a rupture limit of 29% based on the material's elongation, the region with thinning beyond this limit was shorter for triple than for double explosions. These findings highlight the benefits of repeated, especially triple, underwater blasts for improving die filling while controlling thinning in explosive forming.

Keywords: Underwater explosive forming; Female die–forming; Repeated blast loading; Coupled Eulerian–Lagrangian approach; High strain–rate forming.

1. Introduction

In recent, manufacturing techniques related to high strain–rate loading such as dynamic powder compaction, cutting, welding, and forming have been widely employed [1, 2]. After the 1950s, with the growing demand and development of the aviation industry, different types

*Corresponding author.
E-mail address: msadeghy@ihu.ac.ir (Milad Sadegh-Yazdi)

of high–energy rate forming processes were induced and also preferred for shortening the lead times considering equipment and tooling to manufacture complex and large components with axial symmetry in a single operation [3, 4]. Besides, many researchers have proved that the high–energy rate forming effectually improves the formability, reduces the spring–back amount, and promotes an increase in plasticity in lightweight metal alloys [4]. This can be carried out by controlling the forming velocity within an appropriate range. Therefore, high–energy rate forming techniques, namely impact hydroforming (IHF) [5, 6], electrohydraulic forming (EHF) [7, 8], explosive forming [9-11], electromagnetic forming (EMF) [12, 13], etc., in conjunction with high strain rates have recently progressed. In the case of the underwater explosive forming technique [2, 14], repeated and impulsive chemical reactions produce detonation product gasses and high–level energy after triggering the ignition. A high–pressure region with a sharp alteration is generated. Due to the noted advantages, different companies have employed the explosive forming technique to produce space shuttle cones, aircraft radar shields, missile components, nozzles of rocket engines, and boiler products.

According to the noted industrial demands and labor–intensive nature of the explosive forming technique, many scholars have focused on the identification of important processing parameters both numerically and experimentally [15-23]. Akbari Mousavi and his colleagues [24] employed the Zerilli–Armstrong and Johnson–Cook (JC) thermoplasticity models to simulate the dynamic plastic and failure response of circular aluminum plates during the explosive free–forming process. It was found that using the Zerilli–Armstrong equation as the material constitutive model leads to reaching the final deformation shape of the blank in a shorter time. Hadavi et al. [25] used the energy balance method to analytically predict the central deflection of explosively formed cylindrical shells using water and air as media. An accuracy of 84% was obtained for the proposed model. Nishi et al. [26, 27] investigated both experimentally and numerically the explosive die–forming of magnesium alloy plates with a

convex–shaped die at room temperature. In the earlier study [26], due to the steep inclination of the die, racks and wrinkles were observed on the plate surface. Therefore, no good forming was obtained. Later on [27], they changed the arrangement of the explosive charge to control the pressure wave over the plate and allowed the specimen to form in the presence of die inclination. Tanaka et al. [28] suggested a novel efficient approach based on using underwater shockwaves for micropunching the 0.1 mm thick aluminum plates. Multiple circular holes with a diameter of 300 μm on the plate were punched in a single operation. Šunjić and Buljan [29, 30] proposed three different theoretical models to specify the amount of explosive charge mass required for explosive forming of a hemispherical structure with a radius of 95 mm and various wall thicknesses of 3, 4, and 5 mm. It was suggested that the minimum amount of calculated mass should be used in the beginning since changing the type of the detonator (non–electrical, electrical, and electronic) led to different outcomes in terms of explosive charge mass used for experiments. Yildiz [31] numerically studied the influence of different explosive charges of PBXN, Comp–B, HMX, TNT, and PE4 on the formability of copper tubes. The Coupled–Eulerian–Lagrangian (CEL) approach, JC thermoplasticity and damage models, and Jones–Wilkins–Lee (JWL) equations were employed to model large plastic deformation, describe the material behavior, and define the explosive properties, respectively. It was found that the final hardness of the tube was changed by the explosive charge type so that the highest (129.5 HV) and lowest (112.7 HV) hardness values were obtained for the explosive load generated by HMX and TNT, respectively. To employ the idea of using repeated blast loading phenomenon [32-35] in sheet metal forming, Nasiri et al. [36] studied the free–forming of 3 mm thick iron plates under single and repeated underwater blast loads. Compared to single blast loading, better formability, lower von Mises stress distribution, lower amount of JC damage criterion, and excellent smoothness in thickness distribution and deformation profile were found. Later, Yildiz [37] numerically studied the influence of different energy transfer media, including

plasticine, water, and air on the deformation behavior and failure pattern of explosively loaded aluminum tubes. The results indicated that the transfer medium has a significant effect on the final deformation shape, final hardness, and strain rate. The barreling phenomenon as well as the shrinking of the top sections were observed in the plasticine and water media. The highest stress triaxiality and strain rate values were obtained in the air blast loading which decreased the ductility.

As noted above, many experimental studies and numerical simulations presented on the explosive forming technique at room temperature have primarily focused on the large plastic deformation and spring–back behaviors of steel, aluminum alloy, titanium, and copper plates exposed to underwater and air blast loading. Our research team [36] provided a novel concept for the free–forming of metallic plates using the repeated underwater blast loading phenomenon to improve the forming efficiency as well as reduce thinning distribution compared to single loading. However, research studies in the field of repeated blast loading are few and the potential of this processing technique has not yet been investigated for the die–forming of metallic plates. This limits the further applications of repeated explosive forming, therefore, in the current research paper, female die–forming of metallic plates subjected to repeated underwater blast loading is investigated experimentally and numerically. The effects of processing technique parameters such as the number of blast loads and their order, explosive charge mass, and standoff distance on the deformation behavior, deformation velocity, thinning percentage, and die–filling percentage are studied. In summary, sections 2 and 3 describe the experimental procedure and numerical modeling approach, respectively. In section 4, the obtained experimental and numerical results are presented and discussed. The concluding remarks are also noted in section 5.

2. Experimental study

Similar to our previous study [36], 200 mm × 200 mm × 3 mm commercially available Armco® Iron plates with the elemental analysis results given in **Table 1** were used. The test specimen had a thickness of 3 mm.

As shown schematically in **Figure 1**, the test setup was comprised of seven components: a female die, a test plate, a clamping steel frame, a blast tube, an explosive charge, an electrical detonator, and an explosive holder. Note that the blast test was carried out at a secure distance away from the experimental setup. The plate was bolted into the female die with a depth of 20.1 mm and steel square clamping supports. Moreover, it was completely clamped at a radius of 85 mm by seven screws, leaving a circular blast wave–exposed area with a radius of 50 mm in contact with the water. In all experiments, the radius of the die and the radius of the die fillet were 50 mm and 10 mm, respectively. The clamping frame was positioned over the female die. The iron specimen was also mounted to a blast tube made of stainless steel with a height of 300 mm, inner diameter of 100 mm, and outer diameter of 120 mm. The clamping frame, die, and blast tube were considered rigid bodies since they did not experience remarkable permanent plastic deformation compared to the test specimen. The die and clamping frame were made of St–37. Since the explosive charge must remain in the water at a fixed standoff distance (SOD), a 3D–printed holder made of polylactic acid (PLA) was used. By specifying the length of the holder, the standoff distance of the explosive charge from the upper surface of the plate was adjusted to 215 mm. In the present research, a PE4 explosive charge and a 1 g instantaneous electrical detonator were used to create an underwater explosion. The mass of the PE4 explosive charge has been measured by a sensitive scale with an accuracy of 0.01 g. It should be noted that the geometry of the PE4 explosive was in the form of a disk with a diameter of 20 mm and its thickness is proportional to its mass. For repeated blast loads, the already underwater blast-loaded plate was left in the experimental setup and reloaded with the required mass of explosive charge detonated at the same standoff distance.

According to **Table 2**, the explosive charge mass was considered to be 2, 4, 6, 8, and 15 g for test specimens under single underwater blast loading. Meanwhile, for experiments exposed to a double underwater explosion, the charge mass was considered 2 g and 5 g as well as 4 g and 8 g in the 1st and 2nd cycles, respectively. Besides, for experiments exposed to a triple underwater explosion, the charge mass was considered 2 g, 5 g, and 3 g in the 1st, 2nd, and 3rd cycles, respectively. It is worth noting that in all the experiments, the radius of the explosive charge was considered constant and equal to 10 mm. Therefore, the height of the charge was not constant for all experiments due to the changing of its mass. For instance, a taller holder was employed for the explosive charge of 2 g to have the same standoff distance. For repeated loading scenarios, the plate that experienced an underwater explosion once was prepared for testing the second time at the same standoff distance. In **Table 2**, SB, DB, and TB represent single, double, and triple explosions, respectively, and the numbers after them are related to the mass of the explosive charge in each stage of loading. The "," sing was used to separate the mass of explosive charge at each blast loading stage. The letter B is the total number of explosions and the number after that is the explosion number.

3. Numerical simulation methodology

3.1. Simulation approach, equation of states, and constitutive material models

To simulate the die–forming of circular Armco® Iron plates exposed to single and repeated underwater explosions, the Coupled–Lagrangian‑Eulerian (CEL) approach was employed in the ABAQUS commercial finite element solver. The dynamic–explicit analysis was also utilized to activate the Eulerian and Lagrangian combination in the software. This is because the traditional Lagrangian formulation leads to several limitations in modeling the large plastic deformation and failure patterns of the test specimen in explosive sheet metal forming applications. The CEL approach allows the independent movement of the mesh. During the numerical simulation, the Eulerian elements are able to withstand large

deformations without observing any elemental distortion in the mesh [36]. Therefore, the Eulerian domain was utilized for modeling the explosive charge, air, and water. Besides, the Lagrangian mesh was employed for modeling the female die, clamping frame, blast tube, and test plate.

To take into consideration the energy, volume, and pressure behavior of the detonation products during the explosive forming process, the Jones–Wilkins–Lee (JWL) equation of state (EoS) was employed in the hydrodynamic numerical simulations [38]. Furthermore, the ideal gas EoS was used to model the air beneath the test specimen [38]. Since the experimental study was carried out at room temperature, the used parameters in the model were given at 298 ˚K. The Mie–Grüneisen EoS was also utilized for modeling the water based on the linear shock Hugoniot [39, 40]. This can correlate pressure with internal energy and specific volume. The used parameters for noted EoSs in the simulations are represented in **Table 3** [38, 41, 42].

For modeling the mechanical behavior of iron plates exposed to high–strain deformation rates of explosive forming, the Johnson–Cook (JC) strength and damage constitutive models were implemented in the software which considers the yield stress as a function of melting temperature, temperature, strain–rate hardening exponent, strain hardening exponent, and strain [43, 44]. Furthermore, the post–damage–initiation material behavior was also demonstrated by the damage evolution law in the linear form as a function of the equivalent plastic displacement [45]. The used parameters for the JC strength and damage models are represented in **Table 4** [43, 44]. It should be mentioned that the current numerical approach was previously employed by our research group to simulate the free–forming of Armco® Iron plates under single and repeated blast loading. Detailed information regarding the above–mentioned EoSs can be found in Ref. [36].

3.2. Finite element model

To numerically simulate the die–forming of circular plates under repeated underwater blast loading, the ABAQUS/Explicit software package was employed. A dynamic–explicit step was selected in the numerical model due to the rapidity of the process. The CEL approach was also used to realistically simulate the interaction between the test plate, female die, clamping frame, explosive charge, energy transfer medium, and blast tube. Note that the exact geometrical dimensions of noted parts in the experimental study were used to construct the three–dimensional model shown in **Figure 2**.

In the first step, the clamping frame, female die, and blast tube were modeled using discrete three–dimensional quadrilateral rigid elements (R3D4) with a mesh size of 4 mm. The test specimen was modeled using eight–node linear brick elements with reduced integration (C3D8R) and hourglass control with a mesh size of 1 mm × 1 mm × 0.5 mm (six through–thickness elements were considered). Furthermore, it was secured between the female die and the clamping frame along the periphery of the plate. The displacement and rotation of elements on the periphery of the test specimen were constrained to engender fully clamped boundary conditions. Besides, the explosive charge and water were modeled using C3D8R elements with a mesh size of 2 mm. The Eulerian domain was modeled using hexahedral 3D elements with reduced integration (EC3D8R). Its dimensions were also selected in such a way that all other parts were placed inside it. Therefore, a cubic geometry with a square base of 242 mm in length and 334 mm in height with a mesh size of 2 mm was considered as the Eulerian medium. At the end of the modeling, the explosive charge and water were assigned to the Eulerian medium and occupied a fraction of the Eulerian medium according to their position, which is carried out by the Volume Fraction Tool in the ABAQUS/Explicit software. It should be noted that all the noted dimensions were obtained using the mesh sensitivity analysis results.

For the simulation of the contact between the Eulerian and Lagrangian domains, a general contact interaction with a penalty friction coefficient of 0.3 was used. Using general

contact slightly increases the solution time but gives more accurate results. Besides, to define the interaction between the Lagrangian parts of the model, a surface–to–surface contact with hard contact properties and a friction coefficient of 0.3 was used. This simulates the realistic boundary condition allowing for some stretching and sliding in the plate. The clamping frame, female die, and blast tube were completely fixed and their movement and rotation were locked in all directions. Also, no boundary conditions were imposed on the plate and it could slide freely between the die and clamping frame. Moreover, the free outflow boundary condition was assigned to all finite sides of the Eulerian domain, hence, the produced underwater explosion wave propagates freely out of the Eulerian domain with no reflection when it reaches the domain boundaries.

Similar to previous numerical studies presented by our research team [33, 35, 36] and other researchers [46-48] on the repeated loading phenomenon, the repeated underwater blast load was applied to the test specimen in two 1 ms cycles; i.e., the deformation step and the reset event in which the plate was first exposed to the underwater pressure wave in the 1^{st} step for 1 ms, and then the process was followed by a 1 ms reset event in the 2^{nd} step. It is worth mentioning that the time duration of the 1^{st} step is long enough to allow the plate to sufficiently deform. In the 2^{nd} step, called reset event, the load is stopped and followed by an unloading phase which allows the specimen to oscillate under its inertia sufficiently. In addition, the artificial material damping is defined in the numerical model after each blast simulation and between the two consecutive blast events. In this step, the calculation is carried out until the residual elastic vibrations and motion of the model due to the prior blast load cycle vanish. The subsequent blast load cycle is then applied to the specimen for simulation of the repeated blast loading. This process is repeated for the required number of blasts on the specimen while in all restarted analyses, the residual stresses, strains, and deformed shape due to the prior blast load

are preserved by definition of an initial state in the predefined field function of ABAQUS/Explicit.

4. Results and discussion

4.1. Experimental results

The experimental results obtained from the die–forming of metallic plates using underwater explosions along with the cut views of the test specimens are presented in **Table 5** and **Figure 3**. Before analyzing the results of the die–forming process, it should be noted that the 4^{th} explosion does not affect the experimental results obtained in terms of the deformation profile and thinning of the sample. This is similar to our research study [36] on free–forming with repeated underwater explosions. Therefore, only three explosions are enough for die–forming and the test specimen experiences full filling without a noticeable change in thickness.

The maximum permanent deflection, maximum thinning, and die filling are compared in the column chart in **Figure 4**. **Figure 4** shows that single underwater blast loading with the explosive charge mass of 2, 4, 6, 8, and 15 g led to 15.0%, 20.7%, 26.3%, 27.3%, and 36.7% thinning at the central point of the plate which experience the most permanent transverse deformation. Also, for each of the above–mentioned blast loads, the die filling is about 7.6%, 30.0%, 39.0%, 50.9%, and 81.4%. More specifically, by increasing the charge mass from 2 g to 4 g, 6 g, 8 g, and 15 g during the single underwater blast loading, the maximum deflection increased by 8.6%, 7.5%, 6.9%, and 6.4%, the maximum thinning increased by 38.0%, 75.3%, 82.0%, and 144.7%, and the die–filling increased by 2.95, 4.13, 5.70, and 9.71 times. This proves that it is impossible to completely fill the die in the single–stage process of an underwater explosion and it is necessary to apply another load for full filling. The key point is that after the charge mass of 4 g (see the blue elliptical region), the maximum permanent deflection has decreased due to the collision of the test specimen with the bottom of the die and

its reversibility. This issue will be further discussed by presenting numerical simulation results. Moreover, the results experimental showed that using the repeated loading phenomenon (DB–4,8–B2–9) led to 100% die–filling and maximum deflection of 20.1 mm, i.e., the die depth, whereas the obtained maximum thinning of this case was very close to the single loading by 6 g of the explosive charge and less than 8 g. Therefore, more than 4 g of explosive charge should not be chosen at the 1st explosion.

The experimental results in terms of the deformation shape profile, thickness distribution, and thinning along the true and radial distance from the center are depicted in **Figures 5** and **6**. The true distance was calculated from the deformed surface of the plate to the end of its die and clamping support.

The results obtained from the deformation profile of the test specimens in **Figure 5** show that using repeated loading causes the plate to achieve the predetermined shape of the die and the profile of the plate changes from the conical state in the 1st loading to the die shape. In **Figure 6**, it is shown that the underwater explosive forming process leads to the appearance of three green, red, and blue elliptical regions in the thickness distribution (thinning) of the test specimens during loading. As shown in the green region, the minimum thinning belongs to the test specimen under triple underwater explosions with the amount of 2.26 mm which produces a thinning of 24.7%. The obtained result for this case is very close to the test specimen under double underwater explosions of 2 g and 5 g explosive charges with a minimum thickness of 2.28 mm (thinning of 24.0%) since at the 3rd explosion the amount of charge mass is less than the 2nd explosion and under such a circumstance, the central region of the test specimen is not greatly affected and most of the changes are transferred to the areas near the clamped periphery. In general, using an explosive charge mass less than or equal to the charge mass of the previous loading leads to the spring–back phenomenon in the central area, which does not appreciably change the amount of deformation and the thickness of the plate at this region and it directly

affects the die–filling parameter and regions close to clamped periphery. However, the results of the case of DB–4,8–B2–9 are different from DB–2,5–B2–7 since it experiences a greater charge mass in the 2nd load. Compared to SB–4–B1–2, doubling the charge mass in the 2nd loading leads to full die–filling without any significant change in the thinning of the central region. However, it leads to a 29.5% increase in the maximum thinning in the radial distance from the center due to the essence of the repeated loading phenomenon. Note that the maximum thinning at the center belongs to the SB–4–B1–2 test in the case of single loading and increasing the charge mass leads to increasing the thickness distribution. This is because the die does not allow the test specimen to change its shape in proportion to the used charge mass, and the central point quickly reaches the surface of the die and the deformation of the central region is stopped. After that, moving away from the central point and up to a distance of 9 mm from the center of the plate, the maximum thinning still belongs to the TB–2,5,3–B3–12 and the trend does not change. Note that the SB–4–B1–2 test experiences its maximum thinning of 20.7% (2.38 mm) at a distance of 8 mm from the center. The trend changes at a distance of 9 mm from the center and the DB–4,8–B2–9 test undergoes greater thinning due to the doubling of the charge mass in the 2nd loading. Between 15 and 25 mm from the center of the plate, the maximum thinning respectively belongs to SB–15–B1–5 (30.3%, 2.09 mm), TB–2,5,3–B3–12 (28.0%, 2.16 mm), SB–8–B1–4 (27.3%, 2.18 mm), DB–4,8–B2–9 (26.8%, 2.20 mm), SB–6–B1–3 (26.3%, 2.21 mm), DB–2,5–B2–7 (24.3%, 2.27 mm), SB–4–B1–2, (13.3%, 2.60 mm), and SB–2–B1–1 (9.2%, 2.73 mm) in which SB–6–B1–3, SB–8–B1–4, DB–2,5–B2–7, DB–4,8–B2–9, and TB–2,5,3–B3–12 experience their maximum thinning during the whole process. Between 40 and 50 mm from the center of the plate, the trend changes again and the maximum thinning respectively belongs to SB–15–B1–5 (36.7%, 1.90 mm), TB–2,5,3–B3–12 (19.3%, 2.42 mm), DB–2,5–B2–7 (18.3%, 2.45 mm), SB–8–B1–4 (17.7%, 2.47 mm), DB–4,8–B2–9 (17.3%, 2.48 mm), SB–6–B1–3 (10.7%, 2.68 mm), SB–4–B1–2, (6.3%, 2.81 mm), and SB–2–

B1–1 (5.3%, 2.84 mm). By comparing single and repeated underwater explosive loading, it is concluded that the repeated load has led to a significant increase in the thinning of the test specimen near the clamped part of the plate (blue area). This shows that in the repeated test, the effect of the blast wave leads to the development of thinning towards the curved corner of the die so that in addition to die–filling, the maximum thinning occurs before the clamped boundary. Note that it is not possible to achieve full die–filling without using repeated load and maximum thinning occurs in the single loading by increasing the amount of charge mass (SB–15–B1–5). This issue may lead to partial tearing of the plate with a high probability. It is worth noting that one of the advantages of using repeated loading is the reduction of the amount of charge mass to reach the final goal compared to single loading, so the probability of tearing at the clamped boundary becomes lower.

4.2. Validation of the numerical model

To verify the constructed finite element model, the quantitative and qualitative simulation results in terms of the deformation shape profile and thickness distribution are compared with those obtained from underwater explosively loaded circular plates in the experimental study. To this end, a quantitative representation of the thickness distribution in the radial direction of the 3 mm thick plate obtained from experiments and simulations for the case of single (SB–4–B1–2) and repeated (DB–4,8–B2–9) blast loading is shown in **Figure 7**. To better understand and check the accuracy of the model, the error bars (5% and 10%) were used as confidence bands to evaluate the prediction accuracy of the numerical simulation of the process. Great agreement and compatibility were found by comparison of the numerical simulation results and experiments presented for the thickness distribution along the radial direction, therefore, the numerical model has good accuracy in predicting the high strain–rate formability of the Armco® iron plates using the underwater explosive loading technique. More specifically, in the case of single loading, the minimum thickness of 2.38 mm was obtained at

a distance of 8 mm from the center, while the simulation model predicted the plate thickness as 2.30 mm for this point. This indicates the difference between the simulation results and the experimental study is only 3.4% at this critical point. On the other hand, in the case of repeated loading, the plate thickness value at a distance of 23 mm from the center was minimum and obtained as 2.20 mm and 2.07 mm from the experiment and simulation, respectively. Hence, the prediction error is about 7.8%. In general, the measured minimum plate thickness values along with their positions are almost the same as the numerical simulations and the maximum prediction error for both samples is less than 10%. For single loading, the maximum error was created at a distance of 33.5 mm from the center of the plate with a thickness of 2.815 mm from the experiment and a predicted thickness of 2.612 mm. On the other hand, for repeated loading, the maximum error was obtained at a distance of 42 mm from the center of the plate with a thickness of 2.415 mm obtained from experimental studies and a predicted thickness of 2.174 mm. Shortly, it is found that the current numerical model can be used to evaluate the female die–forming of metallic plates subjected to underwater explosive loading for further research with a good confidence level. Note that the main reason for observing slight underestimations or overestimations in experimental and numerical results may be due to the material constants in the JC strength and failure models.

Figure 8 shows the quantitative comparison of the results of the experimental study and numerical simulation for deformation profiles of the test specimens coded SB–4–B1–2 and DB–4,8–B2–9. As shown, the numerical simulation results show a perfect similarity with the experimental studies for the deformation of the plate and there is no significant difference. It is worth noting that the maximum error between simulation and experimental results for the effective parameter of die–filling at the 1st explosive load with a mass charge of 4 g is about 6%. Since the die–filling was 100% in both simulation and experimental studies at the 2nd explosive load, therefore, no error was observed between the simulation and experimental

results of die–filling with a charge of 8 g. In addition, while an area with an incomplete hemispherical shape is created in the 1st loading, in the repeated loading, due to the high pressure produced compared to the 1st loading, the metallic plate sample takes the predetermined shape of the female die. Numerical results also show that the model has a high accuracy in predicting the deformation behavior of the plate for both the real and radial distances from the center to the peripheral boundaries. The most important point here is that, unlike the conventional deep drawing forming process, no wrinkle was found on the skirts of the deformed plate due to the high pressure generated during the forming process, and good surface quality was captured.

4.3. Numerical simulation results

4.3.1. Single explosion

To have a deep study on the die–forming of metallic plates exposed to single underwater explosive loading, the response of Armco® iron plates under different charge masses ranging from 2 to 6 g of PE4 with an interval of 0.5 g was investigated. Note that the charge radius and standoff distance were kept constant as previously. Two important parameters of die–filling and thinning are compared in **Figure 9**. It is shown that the thinning and die–filling parameters indicate single– and double–stage trends, respectively. More specifically, the variation of the maximum thinning in the entire studied interval is just 38% (20.6% to 28.4%). On the other hand, by increasing the charge mass from 2 g to 3.5 g, the die–filling is not noticeable since the metallic plate does not reach the bottom of the die and the corners of the die are filled. However, at the charge mass of 4g, the test specimen touches the bottom of the die and compared to the charge mass of 3.5 g, the die–filling is 2.5 times larger where the thinning does not change significantly. Note that after the charge mass of 4 g, the rate of die–filling remarkably decreases.

Figure 10 shows variations of the deformation shape profile of some selected numerical cases versus the radial distance to better understand how the die–filling parameter changes. It shows that by increasing the charge mass, the test specimen takes the die shape in the corners and central regions, however, the process of approaching the die shape slows down in the middle areas. Besides, it is impossible to increase the charge mass too much in the single explosion forming process since increasing the charge mass greater than 5 g leads to reverse deflection of the central regions (the blue shape at 0 to 3 mm away from the center). Therefore, achieving full die–filling by a single explosion is impossible, as obtained for the case of SB–15–B1 (81.4%) in the experiments. Moreover, for charge masses of less than 4 g, the die–filling is just related to the corners of the die, and the central region takes the die shape at the charge mass of 4 g. This region experiences the reverse deflection phenomenon by increasing the charge mass to 5 g which leads to 34.3% of die–filling, as shown by red shapes.

The variations of the permanent deflection, vertical deformation velocity, and horizontal deformation velocity of the test specimen at the center versus time are presented in **Figures 11** to **13**. The numerical results presented in **Figure 11** indicate that after the charge mass of 3.5 g, the test specimen represents a different behavior and experiences a sensible valley–like area (see the red elliptical region) between the 1st and 2nd peaks due to its collision with the bottom of the die. This becomes larger and larger by increasing the charge mass from 4 g to 6 g due to the large difference between the maximum deformation velocity and return velocity. **Figure 12** indicates that by increasing the charge mass from 2 g to 6 g, the collision velocity (1st peak) and maximum vertical deformation velocity (2nd peak) of the test specimen at the center increase by 48%. However, at the charge mass of 4 g, the slope of both velocity variations changes and decreases for higher charge masses, especially for the collision velocity (32.5%). On the other hand, the return velocity linearly increases by 40% until the charge mass of 4 g and all amounts are less than 21 m/s. However, for higher charge masses, the evolution

of the return velocity does not follow a linear form and it nonlinearly increases to a high amount of 114 m/s (**Table 6**). Under such a circumstance, it can be concluded that achieving full die–filling with lower thinning and using lower charge mass is not possible, as previously proved in the experiments for the case of SB–15–B1–5. **Figure 13** shows that the maximum horizontal deformation velocity reaches 2 m/s at the charge mass of 6 g which is 1.26 and 1.33 times larger than the charge masses of 4 g and 5 g. This proves that the variations of the horizontal deformation velocity are not sensible at the 1st blast, especially for a charge mass of less than 4 g (yellow elliptical region). Therefore, repeated blast loading is required to increase the horizontal deformation and achieve full die–filling.

4.3.2. Double explosion

As noted above, there is no chance of achieving full die–filling by the single underwater explosion technique. Therefore, using repeated loading phenomenon in forming is investigated herein. To this end, the charge masses of 2, 3, 4, and 5 g were used at the 1st blast while the test specimen was again subjected to underwater blast loading by the charge mass of 2 g to 10 g at the 2nd blast. The interval of 2nd loading cycle was considered 1 g. Note that the charge radius and standoff distance were kept constant as previously. Two important parameters of die–filling and thinning are compared in **Figure 14**. The obtained results show that by applying the 2nd underwater blast load, it is possible to experience full–die filling for the case of using 4 g and 8 g charge masses at the 1st and 2nd blasts, respectively. In this case, the specimen experiences a maximum thinning of 32.3%. As shown, in the repeated loading phenomenon, selecting the mass of the explosive charge in each blast plays a key role in achieving the final purpose. For instance, using 3 g and 10 g charge masses at the 1st and 2nd blasts, respectively, does not lead to full–die filling (86.7%) and the plate undergoes a higher thinning (33.8%). However, a high die–filling was achieved compared to the single underwater explosion (Figure **4**). Besides, increasing the charge mass to 5 g and applying the 2nd blast with a charge mass

greater than 5 g is not very effective since it leads to sample tearing. For this case, the maximum die–filling is 75.6% which is lower than a single explosion with a charge mass of 15 g (**Figure 4**).

For better understanding, the variations of two parameters of die–filling and thinning versus the mass of the explosive charge at the 2nd blast are depicted in **Figure 15**. The results show that by increasing the mass of the explosive charge to more than 5 g in the 2nd blast, the linear behavior of maximum thinning changes to a parabolic trend. This is while the die–filling parameter shows a parabolic behavior from the beginning to the end. The fitted functions on the changing trends of both parameters are summarized in **Table 7**. It should be noted that the trend of die–filling parameter variations for the double underwater explosion shows that there is a very low chance of achieving full die–filling by choosing an explosive charge mass of less than 4 g at the 1st explosion. In addition, using 5 g of explosive charge in the 1st explosion and increasing its mass in the 2nd explosion leads to incomplete die–filling and the specimen is torn; therefore, according to the current experimental conditions, the choice of 4 g charge mass for the 1st explosion is quite appropriate.

Considering that reaching full die–filling is one of the goals of the present research study, in the following, numerical simulation results are presented only for those cases where the die–filling is more than 85%, i.e., DB–3,10–B2, DB–4,7–B2, and DB–4,8–B2. **Figure 16** shows variations of the deformation shape profile of the above–noted numerical cases versus the radial distance to better understand the progress of die–filling. It shows that by applying the 2nd blast, the test specimen completely takes the die shape in all regions, however, near the clamped regions (41–50 mm away from the center), there is more compliance between the DB–4,8–B2 and the die profile. Therefore, achieving full die–filling by a double explosion is possible, as obtained for the case of DB–4,8–B2 with lower thinning (32.3%) compared to

others. Note that for other loading conditions, there is no possibility of achieving full die–filling in a double–step process and middle regions cannot match the die profile.

The variations of the permanent deflection, vertical deformation velocity, and horizontal deformation velocity of the test specimen at the center versus time are presented in **Figures 17** to **19** in the smooth condition. **Figure 17** indicates that test specimens under repeated loading experience a reverse deflection at 1.2 ms (see the red circular region and enlarged view) since the 2nd load is much stronger than the first one and it leads to collision with the bottom of the die. This becomes larger and larger by increasing the 2nd charge mass to 10 g for the case of DB–3,10–B2. However, this does not affect the final response of the plate and it greatly takes the profile of the die at the end of the process for the case of DB–4,8–B2. **Figures 18** and **19** represent that repeated loading significantly affects the horizontal and vertical deformation velocity in comparison to those obtained by a single explosion. For the case of DB–4,8–B2, the maximum values of the horizontal and vertical deformation velocity are 72.7 m/s and 18.9 m/s leading to full die–filling. At the 1st blast, most of the plastic work is mainly spent on the vertical deformation and the test specimen takes almost the profile of the die at a distance of 0–10 mm from the center. For this, the vertical deformation velocity greatly reduces at the 2nd blast and the variations of the horizontal deformation velocity are remarkably sensible. Comparing the results obtained for DB–3,10–B2 and DB–4,7–B2 shows that there is no direct relationship between the maximum values of the deformation velocity and full–die filling since the first case experiences smaller die–filling and larger deformation velocity, therefore, selecting an optimized charge mass for each blast plays a key role to achieve the noted goals.

4.3.3. Triple explosion

Using the idea of a double underwater blast explosion showed that there is only one rational chance to achieve full die–filling (DB–4,8–B2). Note that other successful conditions for the double explosion phenomenon are not applicable since it is required to use more explosive charge mass which leads to higher thinning. Therefore, the number of blasts was increased to find more cases and the results of the triple explosion are presented and discussed herein. This helps us to decrease the explosive charge in each loading stage and prevent higher thinning without changing the deformation shape profile and die-filling parameter. Under such a circumstance, there are 44 cases with full–die filling conditions and different thinnings, however, 6 cases, i.e., TB–2,5,3, TB–2,6,2, TB–3,4,3, TB–3,5,2, TB–3,5,3, and TB–5,4,2 have been selected herein to discuss due to experiencing less thinning and requiring less explosive charge mass to apply.

The variations of deformation shape profile and thinning versus the radial distance are depicted in **Figure 20**. The results show that the test specimen takes the die shape in all regions very well and there are no inconsistencies with the die profile. Besides, the obtained results for thinning indicate that the lowest value for the maximum thinning parameter belongs to the case of TB–2,5,3–B3 in comparison to other cases subjected to triple explosion. This is the fact that the tested specimen under double explosion experiences less thinning at the center (24.0%). Of course, this issue is not a good criterion to compare the results obtained for the two cases of DB–4,8–B2 and TB–2,5,3–B3 since the amount of thinning of the tested specimen changes along the radial distance from the plate center. To accurately answer this problem, a rupture limit of 29% was determined according to the elongation of the used material. It is shown that the length of the black grids (1.0 mm × 0.5 mm) in which the tested specimen is exposed to double explosion is much larger than the yellow grids. The lengths of noted colored cubes are respectively 11.7% and 15.8% of the total length which undergo thinning of more than 29%. Note that the length of green grids was not considered for the double–blast–loaded specimen

since under such a circumstance, the plate experiences higher thinning exposed to the triple explosion. Besides, purple and black grids are where there is a large difference between the thinning of double and triple–blast–loaded specimens. This proves the advantage of forming with triple explosion over double.

Since the specimen exposed to the triple explosion has taken the die profile completely, the central deflection of the plate during the 3rd blast is just shown in **Figure 21** to compare its fluctuation for different loading conditions. Since the explosive charge masses of the 1st and 2nd blasts differ greatly, the tested specimen (TB–2,5,3–B2) experiences considerable plastic deformation during the 2nd stage of loading. At the 3rd stage of loading, all cases did not undergo any significant fluctuation, therefore, it is important to choose the lowest explosive charge mass (2+5+3 g) for forming, i.e., TB–2,5,3.

The variations of the vertical and horizontal deformation velocity of the test specimen at the center versus time are presented in **Figures 22** and **23** in the smooth condition, respectively. No rational trend was observed at the 3rd blast for both deformation velocities since the charge mass is less than the previous loading (2nd blast) in all cases. The vertical and horizontal deformation velocities are just sensible for the case of TB–2,5,3 and TB–2,6,2, therefore, applying the 3rd blast is applicable under such a circumstance. Besides, the variation of deformation velocity is more highlighted for the case of TB–2,5,3 in comparison to TB–2,6,2 and can be considered as the best testing condition for forming by the triple explosion phenomenon. To provide a quantitative comparison of the deformation response at the plate center under triple explosion loading, the numerical results of the deformation velocity are summarized in **Table 8**.

4.3.4. Further discussion

According to the above results and discussion, the numerical simulation results obtained for two cases DB–4,8 and TB–2,5,3 in terms of the Von Mises stress (S Mises), equivalent plastic strain (PEEQ), and JC damage initiation criterion (JCCRT) are further discussed herein to determine which one provides better conditions for metal sheet forming using repeated loading phenomenon. **Figures 24** to **26** respectively represent the noted results with a constant legend at the last loading cycle for each sequence of simulation time frame. The obtained simulation results for the Von Mises stress show that the DB–4,8–B2 specimen experiences higher stress during the forming process and there is no red region on both the front and back views of the specimen exposed to triple underwater blast loading. It is noteworthy to mention that the highest value of stress experienced in the green region is 0.67 times that of the red region. This problem can be mentioned as an achievement in the process of forming with repeated explosions, in which increasing the number of explosions leads to the loss of high levels of stress in the boundary and central regions of the plate. This result was also observed for the other two outputs, i.e., equivalent plastic strain and JC damage initiation criterion, in **Figures 25** and **26**, with the difference that at the beginning of the last loading cycle, the testing specimen under three consecutive explosions suffers higher values, but at the end of the process, the red regions become green or yellow with lower values.

5. Conclusion

In this paper, to overcome the difficulties of explosive forming by a single explosion, the idea of using repeated loading phenomenon on the formability of Armco® Iron was experimentally and numerically evaluated. To this end, twelve experiments for eight different case studies (5 for a single explosion, 2 for a double explosion, and 1 for a triple explosion) were carried out and experimental results in thinning and die–filling percentages were compared. Selecting the mass of the explosive charge in each blast plays a key role in achieving the final purpose, i.e., full die–filling with the lowest thinning, therefore, a rigorous numerical simulation in

ABAQUS/Explicit software was performed. Based on the conducted experiments and numerical simulations, the following conclusions can be drawn:

- In a single explosion, the test specimen takes the die shape in the corners and central regions by increasing the charge mass, however, the process of approaching the die shape slows down in the middle areas. Besides, increasing the charge mass leads to reverse deflection of the central regions. On the other hand, the variations of the horizontal deformation velocity are not sensible at the 1st blast. Therefore, there is no chance of achieving full die–filling with a single underwater explosion technique. The maximum die–filling by a single explosion was 81.4%.
- It is possible to achieve full die–filling by using lower explosive charge mass in a double–step process. Under such a circumstance, middle and corner regions can match the die profile.
- Using an explosive charge mass less than or equal to the charge mass of the previous loading leads to the spring–back in the central area, which does not appreciably change the amount of deformation and the thickness of the plate at this region and it directly affects the die–filling parameter and regions close to clamped periphery.
- Repeated loading significantly affects the horizontal and vertical deformation velocity in comparison to a single explosion. At the 1st blast, most of the plastic work is mainly spent on the vertical deformation and the test specimen takes almost the profile of the central region. For this, the vertical deformation velocity greatly reduces at the 2nd blast and the variations of the horizontal deformation velocity are remarkably sensible.
- Using the idea of a double underwater blast explosion showed that there is only one rational chance to achieve full die–filling (DB–4,8–B2) and other conditions for the double explosion phenomenon are not applicable since it requires to use of more explosive charge mass which leads to higher thinning. However, 44 cases with full–die

filling conditions and different thinnings were obtained for the triple explosion. This helps the user to select the best condition based on his/her needs.

- A rupture limit of 29% was determined according to the elongation of the used material to see the superiority of triple explosion over double. It was found that compared to the double explosion, the length of the plate that experiences thinning greater than the determined rupture limit is shorter in the triple explosion.
- Using repeated loading and increasing the number of explosions leads to the loss of high levels of stress, equivalent plastic strain, and JC damage initiation criterion in the boundary and central regions of the plate.

Acknowledgements Not applicable.

Author contributions Conceptualization, H.K., M.S., M.Z., T.M.M; methodology, M.K.; formal analysis, M.K.; data curation, M.K.; writing—original draft preparation, T.M.M, T.P.; review and editing, T.M.M; supervision, H.K., M.S., M.Z., T.M.M. All authors have read and agreed to the published version of the manuscript.

Funding Not applicable.

Data availability Not applicable.

Code availability Not applicable.

6. Declarations

Ethics approval Not applicable.

Consent to participate Not applicable.

Consent for publication All authors have agreed to authorship, read, and approved the manuscript, and given consent for submission and subsequent publication of the manuscript.

The authors guarantee that the contribution to the work has not been previously published elsewhere.

Conflicts of interest The authors declare no conflict of interest.

7. References

[1] R. Rajendran, K. Narasimhan, Damage prediction of clamped circular plates subjected to contact underwater explosion, International Journal of Impact Engineering, 25 (2001) 373–386.

[2] R. Rajendran, K. Narasimhan, Deformation and fracture behaviour of plate specimens subjected to underwater explosion—a review, International Journal of Impact Engineering, 32 (2006) 1945–1963.

[3] N. Gupta, Response of thin walled metallic structures to underwater explosion: A review, International Journal of Impact Engineering, 156 (2021) 103950.

[4] T.Z. Blazynski, Explosive welding, forming and compaction, Springer Science & Business Media, 2012.

[5] Y. Ma, S.–f. Chen, D.–y. Chen, D. Banabic, H.–w. Song, Y. Xu, S.–h. Zhang, X.–s. Fan, Q. Wang, Determination of the forming limit of impact hydroforming by frictionless full zone hydraulic forming test, International Journal of Material Forming, 14 (2021) 1221–1232.

[6] A. Mohseni, J. Rezapour, S. Gohari Rad, R. Rajabiehfard, Low velocity impact tube hydroforming process: experiments and FSI modeling by considering ductile damage model, International Journal of Material Forming, 16 (2023) 62.

[7] M. Zohoor, S.M. Mousavi, Experimental analysis and smoothed particle hydrodynamics modeling of electrohydraulic forming of sheet metal parts, Journal of Manufacturing Processes, 35 (2018) 16–28.

[8] A.V. Mamutov, S.F. Golovashchenko, V.S. Mamutov, J.J. Bonnen, Modeling of electrohydraulic forming of sheet metal parts, Journal of Materials Processing Technology, 219 (2015) 84–100.

[9] D. Kakogiannis, P. Verleysen, B. Belkassem, F. Coghe, L. Rabet, Multiscale modelling of the response of Ti–6AI–4V sheets under explosive loading, International Journal of Impact Engineering, 119 (2018) 1–13.

[10] T.M. Mostofi, H. Babaei, M. Alitavoli, G. Lu, D. Ruan, Large transverse deformation of double–layered rectangular plates subjected to gas mixture detonation load, International Journal of Impact Engineering, 125 (2019) 93–106.
[11] D. Giuliano, L. Lomazzi, M. Giglio, A. Manes, On Eulerian–Lagrangian methods to investigate the blast response of composite plates, International Journal of Impact Engineering, 173 (2023) 104469.
[12] S.D. Kore, P. Date, S. Kulkarni, Effect of process parameters on electromagnetic impact welding of aluminum sheets, International Journal of Impact Engineering, 34 (2007) 1327–1341.
[13] A.–C. Jeanson, F. Bay, N. Jacques, G. Avrillaud, M. Arrigoni, G. Mazars, A coupled experimental/numerical approach for the characterization of material behaviour at high strain–rate using electromagnetic tube expansion testing, International Journal of Impact Engineering, 98 (2016) 75–87.
[14] H. Iyama, A. Kira, M. Fujita, S. Kubota, K. Hokamoto, S. Itoh, An investigation on underwater explosive bonding process, Journal of Pressure Vessel Technology, 123 (2001) 486–492.
[15] W. Huang, B. Jia, W. Zhang, X. Huang, D. Li, P. Ren, Dynamic failure of clamped metallic circular plates subjected to underwater impulsive loads, International Journal of Impact Engineering, 94 (2016) 96–108.
[16] J. LeBlanc, C. Shillings, E. Gauch, F. Livolsi, A. Shukla, Near field underwater explosion response of polyurea coated composite plates, Experimental Mechanics, 56 (2016) 569–581.
[17] W. Huang, W. Zhang, X. Huang, X. Jiang, Y. Li, L. Zhang, Dynamic response of aluminum corrugated sandwich subjected to underwater impulsive loading: experiment and numerical modeling, International Journal of Impact Engineering, 109 (2017) 78–91.
[18] Z. Zhang, C. Wang, L. Wang, A. Zhang, V.V. Silberschmidt, Underwater explosion of cylindrical charge near plates: Analysis of pressure characteristics and cavitation effects, International Journal of Impact Engineering, 121 (2018) 91–105.
[19] H. Iyama, Y. Higa, M. Nishi, S. Itoh, Magnesium alloy forming using underwater shock wave by wire electric discharge, International Journal of Multiphysics, 13 (2019) 269–282.
[20] N. Maharjan, W. Zhou, Y. Zhou, N. Wu, Underwater laser hardening of bearing steels, Journal of Manufacturing Processes, 47 (2019) 52–61.
[21] P. Ren, C. Ding, Y. Liu, R. Ye, J. Wu, Y. Ma, W. Zhao, W. Zhang, Dynamic response and failure of carbon/epoxy composite sandwich subjected to underwater impulsive loading, International Journal of Impact Engineering, 143 (2020) 103614.

[22] C. Javier, M. Galuska, M. Papa, J. LeBlanc, H. Matos, A. Shukla, Underwater explosive bubble interaction with an adjacent submerged structure, Journal of Fluids and Structures, 100 (2021) 103189.
[23] Z. Liu, X. Luo, X. He, J. Liu, S. Yu, W. Huang, The dynamic response of composite auxetic re–entrant honeycomb structure subjected to underwater impulsive loading, International Journal of Impact Engineering, (2024) 104999.
[24] S.A. Mousavi, M. Riahi, A.H. Parast, Experimental and numerical analyses of explosive free forming, Journal of Materials Processing Technology, 187 (2007) 512–516.
[25] V. Hadavi, J. Zamani Ashani, A. Mozaffari, Theoretical calculation of the maximum radial deformation of a cylindrical shell under explosive forming by a new energy approach, Proceedings of the Institution of Mechanical Engineers, Part C: Journal of Mechanical Engineering Science, 226 (2012) 576–584.
[26] M. Nishi, H. Sakaguchi, S. Tanaka, H. Iyama, M. Fujita, Research on explosive forming of magnesium alloy plate using numerical simulation and experimental studies (I), Science and Technology of Energetic Materials, 79 (2018) 156–159.
[27] M. Nishi, H. Sakaguchi, S. Tanaka, H. Iyama, M. Fujita, Research on explosive forming of magnesium alloy plate using numerical simulation and experimental studies (II), Science and Technology of Energetic Materials, 82 (2021) 39–43.
[28] S. Tanaka, I. Bataev, M. Nishi, I. Balagansky, K. Hokamoto, Micropunching large–area metal sheets using underwater shock wave: Experimental study and numerical simulation, International Journal of Machine Tools and Manufacture, 147 (2019) 103457.
[29] D. Šunjić, S. Buljan, Determining the amount of explosives in metal forming, in: Proceedings of the 30th DAAAM International Symposium, 2019, pp. 0592–0598.
[30] D. Šunjić, S. Buljan, Explosive Forming: Analytical Methods for Determining the Mass of Explosives, Advanced Technologies and Materials, 48 (2023) 9–12.
[31] R.A. Yildiz, Investigation of the explosive type on the high strain forming of OFHC copper tube, The Journal of Strain Analysis for Engineering Design, 57 (2022) 266–278.
[32] T.F. Henchie, S.C.K. Yuen, G. Nurick, N. Ranwaha, V. Balden, The response of circular plates to repeated uniform blast loads: An experimental and numerical study, International Journal of Impact Engineering, 74 (2014) 36–45.
[33] M. Rezasefat, T.M. Mostofi, T. Ozbakkaloglu, Repeated localized impulsive loading on monolithic and multi–layered metallic plates, Thin–Walled Structures, 144 (2019) 106332.

[34] M. Ziya–Shamami, H. Babaei, T.M. Mostofi, H. Khodarahmi, Structural response of monolithic and multi–layered circular metallic plates under repeated uniformly distributed impulsive loading: An experimental study, Thin–Walled Structures, 157 (2020) 107024.
[35] M. Behtaj, H. Babaei, T.M. Mostofi, Repeated uniform blast loading on welded mild steel rectangular plates, Thin–Walled Structures, 178 (2022) 109523.
[36] S. Nasiri, M. Sadegh–Yazdi, S. Mousavi, M. Ziya–Shamami, T. Mostofi, Repeated underwater explosive forming: Experimental investigation and numerical modeling based on coupled Eulerian–Lagrangian approach, Thin–Walled Structures, 172 (2022) 108860.
[37] R.A. Yildiz, A numerical investigation on the effect of transfer medium in explosive forming, The International Journal of Advanced Manufacturing Technology, 126 (2023) 3249–3265.
[38] S.E. Rigby, A. Tyas, T. Bennett, S.D. Fay, S.D. Clarke, J.A. Warren, A numerical investigation of blast loading and clearing on small targets, International Journal of Protective Structures, 5 (2014) 253–274.
[39] S. Avachat, M. Zhou, Effect of facesheet thickness on dynamic response of composite sandwich plates to underwater impulsive loading, Experimental Mechanics, 52 (2012) 83–93.
[40] S. Avachat, M. Zhou, Compressive response of sandwich plates to water–based impulsive loading, International Journal of Impact Engineering, 93 (2016) 196–210.
[41] T. Tetik, R. Yildiz, A. Labanieh, B. Yoruk, S. Kursun Bahadir, F. Kalaoglu, V. Koncar, Hydrodynamic modeling of e–textile fabric washing behavior by the Coupled Eulerian–Lagrangian method, Textile Research Journal, (2020) 0040517520973455.
[42] H. Iyama, Y. Higa, M. Nishi, S. Itoh, Numerical simulation of explosive forming using detonating fuse, The International Journal of Multiphysics, 11 (2017) 233–244.
[43] G.R. Johnson, W.H. Cook, A constitutive model and data for metals subjected to large strains, high strain rates and high temperatures, in: Proceedings of the 7th International Symposium on Ballistics, The Netherlands, 1983, pp. 541–547.
[44] G. Johnson, W. Cook, Fracture characteristics of three metals subjected to various strains, strain rates and temperatures and pressures, Engineering Fracture Mechanics, 21 (1985) 31–48.
[45] P.M. Elek, S.S. Jaramaz, D.M. Micković, N.M. Miloradović, Experimental and numerical investigation of perforation of thin steel plates by deformable steel penetrators, Thin–Walled Structures, 102 (2016) 58–67.
[46] S.–R. Cho, D.D. Truong, H.K. Shin, Repeated lateral impacts on steel beams at room and sub–zero temperatures, International Journal of Impact Engineering, 72 (2014) 75–84.

[47] D.D. Truong, H.K. Shin, S.–R. Cho, Permanent set evolution of aluminium–alloy plates due to repeated impulsive pressure loadings induced by slamming, Journal of Marine Science and Technology, 23 (2018) 580–595.
[48] D.D. Truong, H.K. Shin, S.–R. Cho, Repeated lateral impacts on steel grillage structures at room and sub–zero temperatures, International Journal of Impact Engineering, 113 (2018) 40–53.

Table 1. Chemical composition of the Armco® Iron material used in this study

Element	**C**	**Mn**	**P**	**S**	**Cu**	**N**
Amount (wt%)	0.006	0.060	0.004	0.005	0.011	0.004
Element	**Si**	**Al**	**Cr**	**Mo**	**Ni**	**Sn**
Amount (wt%)	0.004	0.005	0.024	0.003	0.018	0.001

Table 2. Testing groups

Test code	Total number of loads	Blast number	Charge mass (g)
SB–2–B1–1	1	1	2
SB–4–B1–2	1	1	4
SB–6–B1–3	1	1	6
SB–8–B1–4	1	1	8
SB–15–B1–5	1	1	15
DB–2,5–B1–6	2	1	2
DB–2,5–B2–7		2	5
DB–4,8–B1–8	2	1	4
DB–4,8–B2–9		2	8
TB–2,5,3–B1–10	3	1	2
TB–2,5,3–B2–11		2	5
TB–2,5,3–B3–12		3	3

Table 3. Parameters of employed EoSs in the numerical simulation [38, 41, 42]

Material	**EoS**	**Parameters**							
PE4	JWL	ρ_0	D	E_0	A	B	R_1	R_2	ω
		(kg/m^3)	(m/s)	(J/m^3)	(GPa)	(GPa)	–	–	–
		1601	8193	9000	609.8	12.95	4.5	1.4	0.25
Air	Ideal gas	ρ	R	P_A	T_z	T_0	C_v		
		(kg/m^3)	(J/kgK)	(kPa)	(K)	(K)	(J/kgK)		
		1.293	287	101.325	0	288.4	1003.5		
Water	Mie–Grüneisen	ρ_0	C_0	μ	s	Γ_0			
		(kg/m^3)	(m/s)	(N·s/m^2)	–	–			
		1000	1490	0.001	1.79	1.65			

Table 4. The JC material and failure model constant parameters [43, 44]

Material properties	**Notations**	**Unit**	**Armco® Iron**
Modulus of Elasticity	E	GPa	207
Poisson's ratio	υ	–	0.29
Density	ρ	kg/m^3	7890
Yield stress and strain hardening	A	MPa	175
	B	MPa	360
	n	–	0.32
Strain rate hardening	$\dot{\varepsilon}_0$	s^{-1}	1.0
	C	–	0.06
Temperature softening	T_0	K	298
	T_{melt}	K	1811
	m	–	0.55
Specific heat	C_p	J/kgK	452
Fracture strain constant	D_1	–	–2.20
	D_2	–	5.43
	D_3	–	–0.47
	D_4	–	0.016
	D_5	–	0.63

Table 5. Experimental results

Test code	Maximum Deflection (mm)	Maximum thinning (%)	Die–filling (%)
SB–2–B1–1	18.60	15.0	7.6
SB–4–B1–2	20.02	20.7	30.0
SB–6–B1–3	19.99	26.3	39.0
SB–8–B1–4	19.89	27.3	50.9
SB–15–B1–5	19.79	36.7	81.4
DB–2,5–B2–7	20.10	24.3	60.2
DB–4,8–B2–9	20.10	26.8	100
TB–2,5,3–B3–12	20.10	28.0	100

Table 6. Numerical simulation results obtained for the deformation velocity at the center by a single explosion

Case code	Vertical velocity (m/s)			Horizontal velocity (m/s)	
	Collision	Maximum	Return	Collision	Maximum
SB–2–B1	106	132	15	∼0	0.5
SB–2.5–B1	111	142	16	–	–
SB–3–B1	120	150	18	∼0	0.8
SB–3.5–B1	131	159	19	–	–
SB–4–B1	136	168	21	0.35	1.5
SB–4.5–B1	140	175	38	–	–
SB–5–B1	146	182	47	0.45	1.6
SB–5.5–B1	152	189	97	–	–
SB–6–B1	157	196	114	0.6	2.0

Table 7. Fitted functions to predict the maximum thinning and die–filling parameters in the double explosion forming process

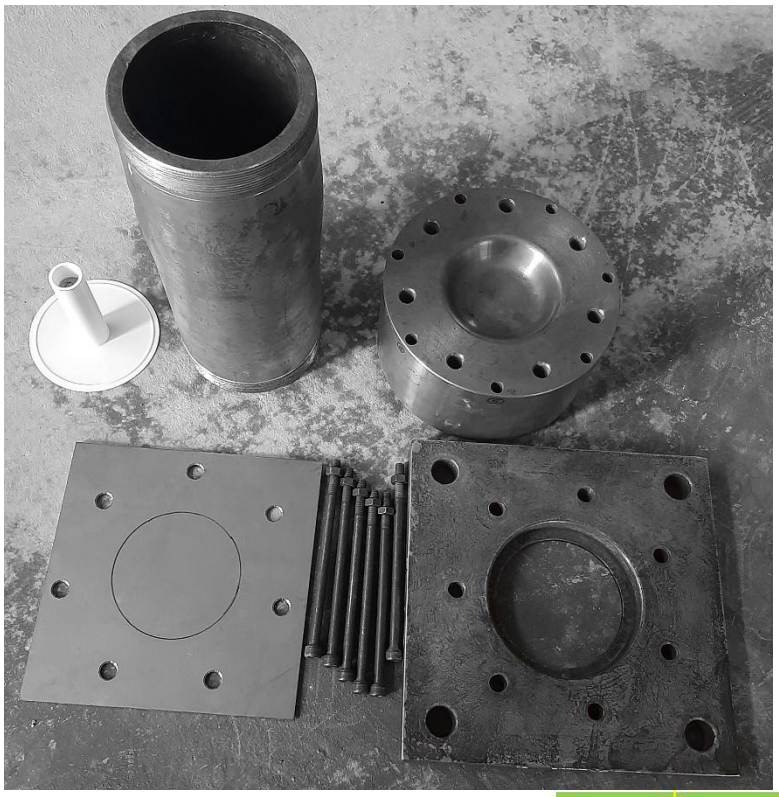
Case code	Maximum thinning (%)		Die–filling (%)	
	Function (1st step) **Function (2nd step)**	**R^2**	**Function**	**R^2**
SB–2	$y = 2.04x + 16.5$ –	0.970 –	$y = 1.19x^2 + 1.85x - 2.92$	0.897
DB–2	$y = 1.42x + 21.0$ $y = 0.11x^2 - 0.80x + 29.6$	0.990 0.963	$y = -0.42x^2 + 10.8x + 11.0$	0.995
DB–3	$y = 1.31x + 23.1$ $y = 0.10x^2 - 0.62x + 30.0$	0.998 0.981	$y = -0.48x^2 + 12.1x + 12.9$	0.995
DB–4	$y = 0.98x + 25.8$ $y = 0.15x^2 - 1.31x + 33.4$	0.969 0.960	$y = -0.17x^2 + 12.4x + 12.7$	0.992
DB–5	$y = 0.88x + 27.5$ –	0.984 –	$y = 1.40x^2 + 0.27x + 39.5$	0.998

Table 8. Numerical simulation results obtained for the deformation velocity at the center by a triple explosion

Case code	Vertical velocity (m/s)			Horizontal velocity (m/s)	
	1st Peak	2nd Peak	Return	Maximum	Return
TB–2,5,3–B2	73 (0.16 ms)	35 (0.23 ms)	19 (0.19 ms)	2.6 (0.23 ms)	1.5 (0.22 ms)
TB–2,6,2–B2	94 (0.16 ms)	81 (0.23 ms)	27 (0.41 ms)	4.4 (0.23 ms)	4.7 (0.22 ms)
TB–3,4,3–B2	11 (0.14 ms)	46 (0.24 ms)	41 (0.25 ms)	1.0 (0.27 ms)	1.3 (0.26 ms)
TB–3,5,2–B2	19 (0.14 ms)	87 (0.24 ms)	24 (0.19 ms)	4.1 (0.25 ms)	1.6 (0.31 ms)
TB–5,4,2–B2	5 (0.14 ms)	34 (0.23 ms)	19 (0.21 ms)	2.7 (0.24 ms)	0.7 (0.29 ms)
TB–2,5,3–B3	37* (0.30 ms)	7* (0.52 ms)	15 (0.18 ms)	6.1 (0.21 ms)	4.6 (0.20 ms)
TB–2,6,2–B3	8* (0.27 ms)	9* (0.45 ms)	18 (0.25 ms)	3.5 (0.33 ms)	1.6 (0.16 ms)
TB–3,4,3–B3	25* (0.18 ms)	34* (0.20 ms)	17 (0.19 ms)	0.6 (0.16 ms)	4.6 (0.18 ms)
TB–3,5,2–B3	10* (0.31 ms)	15* (0.36 ms)	14 (0.24 ms)	1.6 (0.32 ms)	2.1 (0.37 ms)
TB–3,5,3–B3	22* (0.21 ms)	12* (0.35 ms)	7 (0.18 ms)	1.6 (0.35 ms)	1.8 (0.29 ms)
TB–5,4,2–B3	15* (0.24 ms)	12* (0.47 ms)	10 (0.04 ms)	2.3 (0.16 ms)	0.8 (0.53 ms)

*: Due to many fluctuations, the two peaks with the highest values are reported.

(a)



(b)

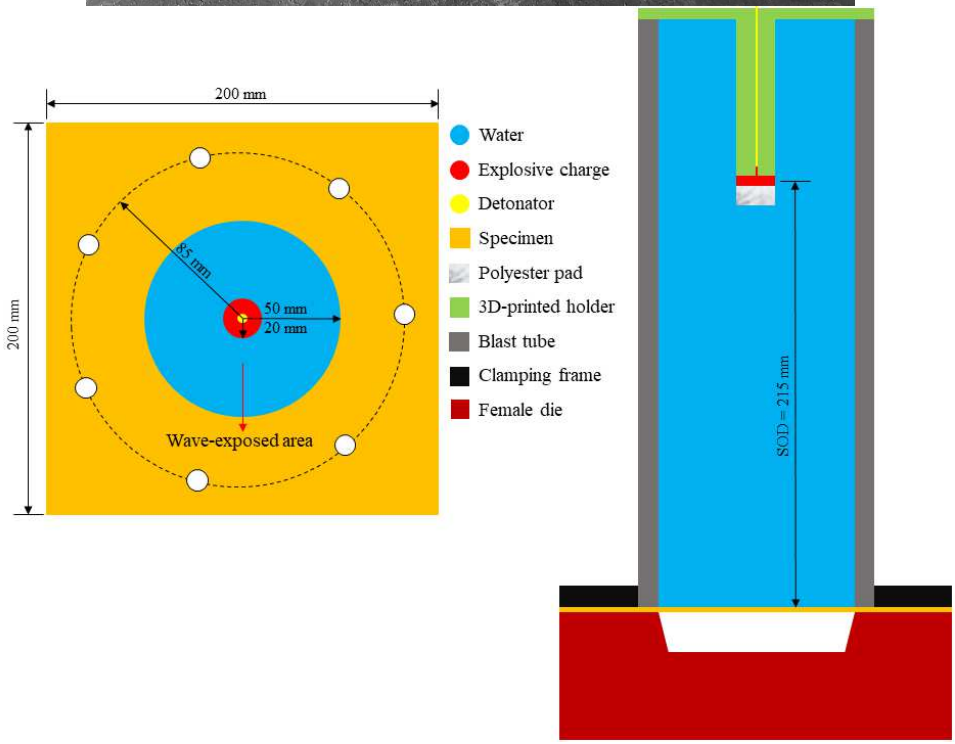


Figure 1. Underwater explosive forming: a) Experimental testing setup; b) schematic of the cross–sectional view.

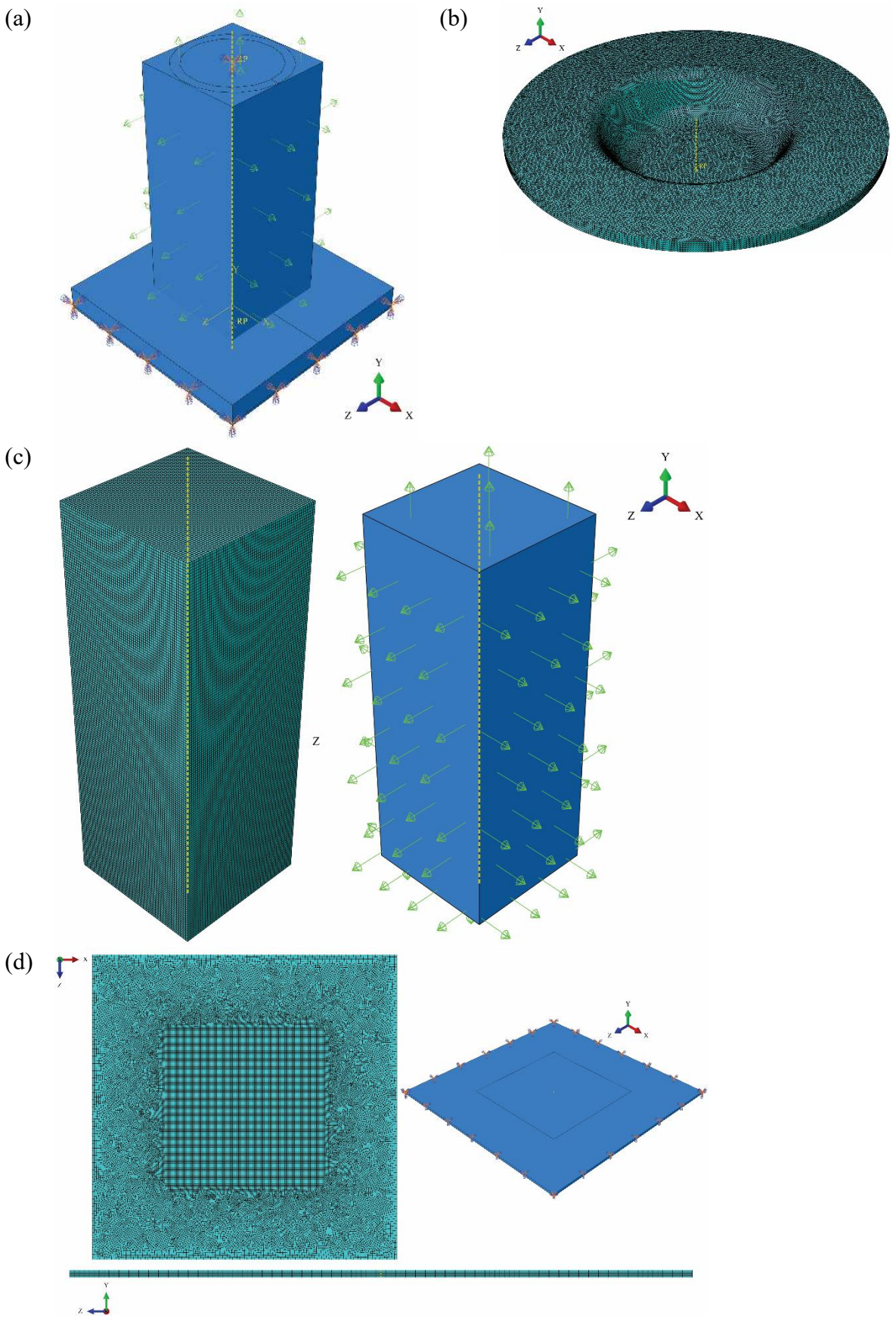


Figure 2. Finite element model of the underwater explosive forming: a) assembly and boundary conditions; b) female die; c) Eulerian domain; d) test specimen.

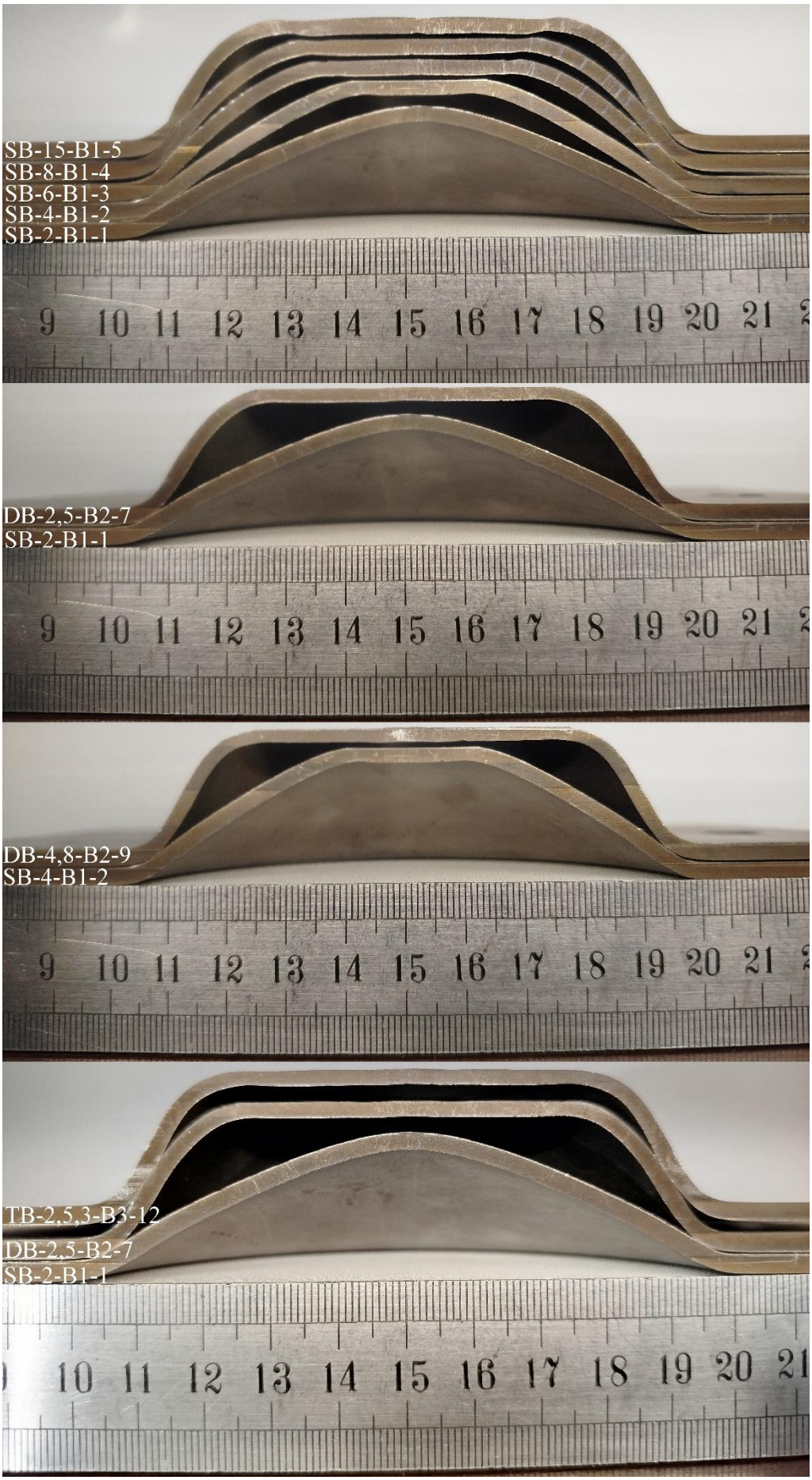


Figure 3. Cut views of the test specimens.

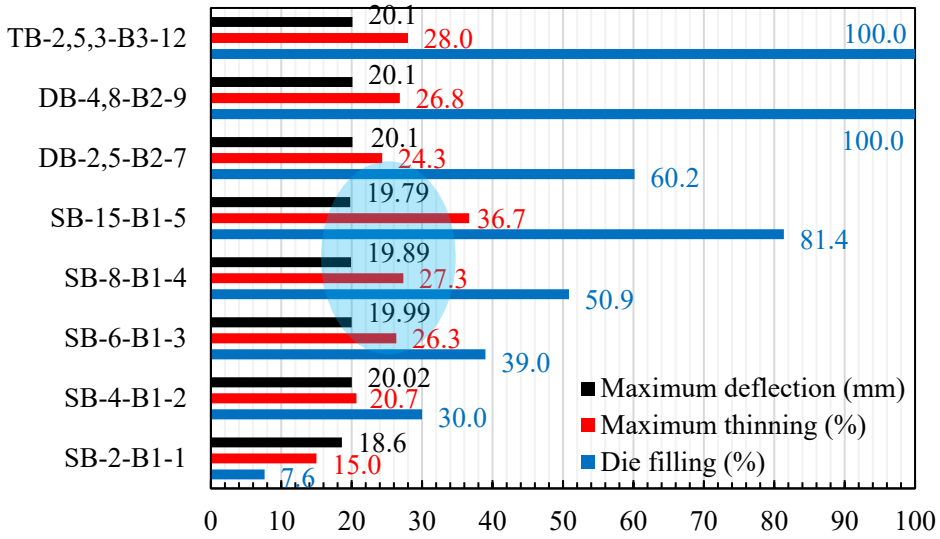


Figure 4. Experimental results in column charts.

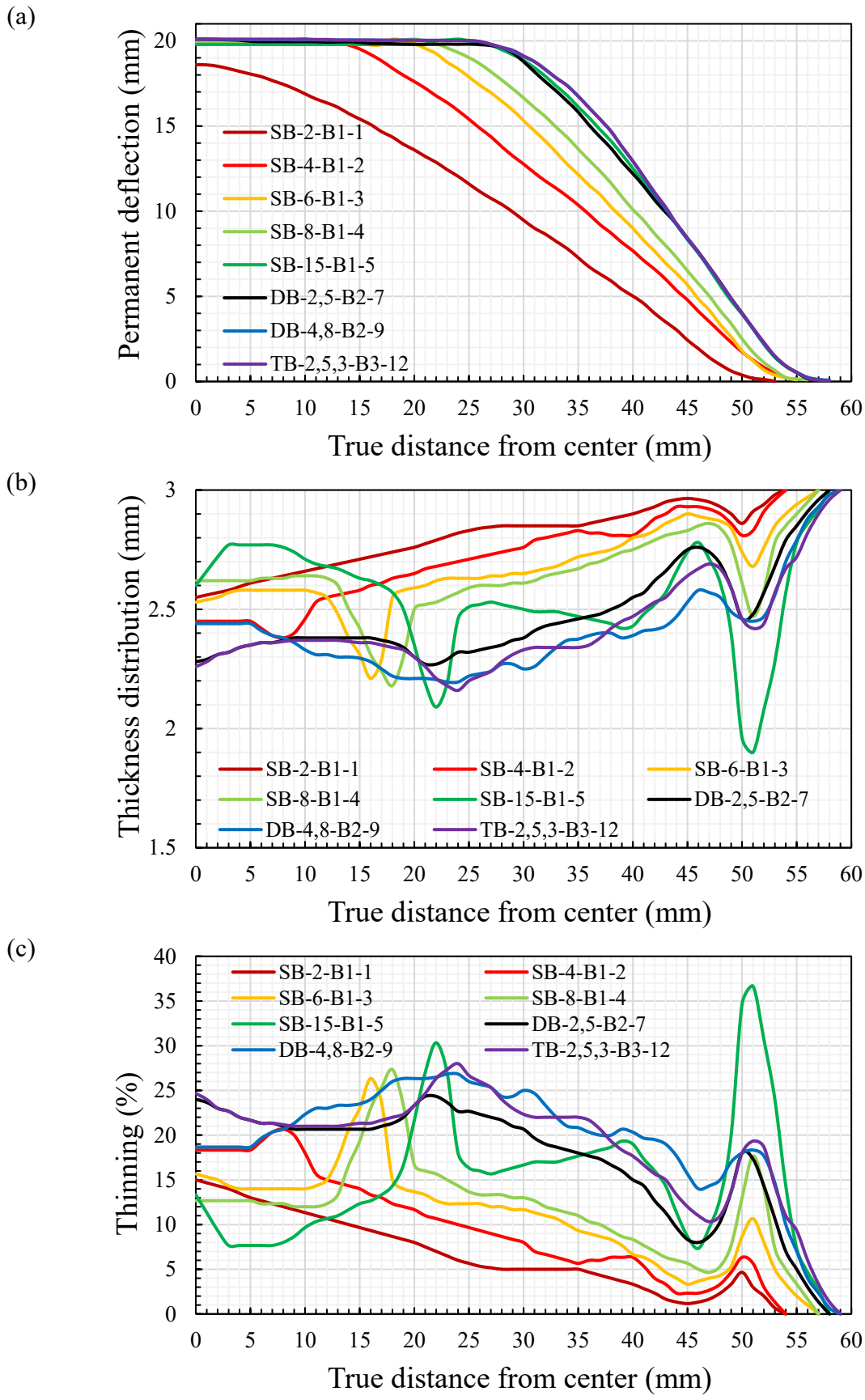


Figure 5. Experimental results along the true distance from the center: a) Deformation shape profile; b) thickness distribution; c) thinning.

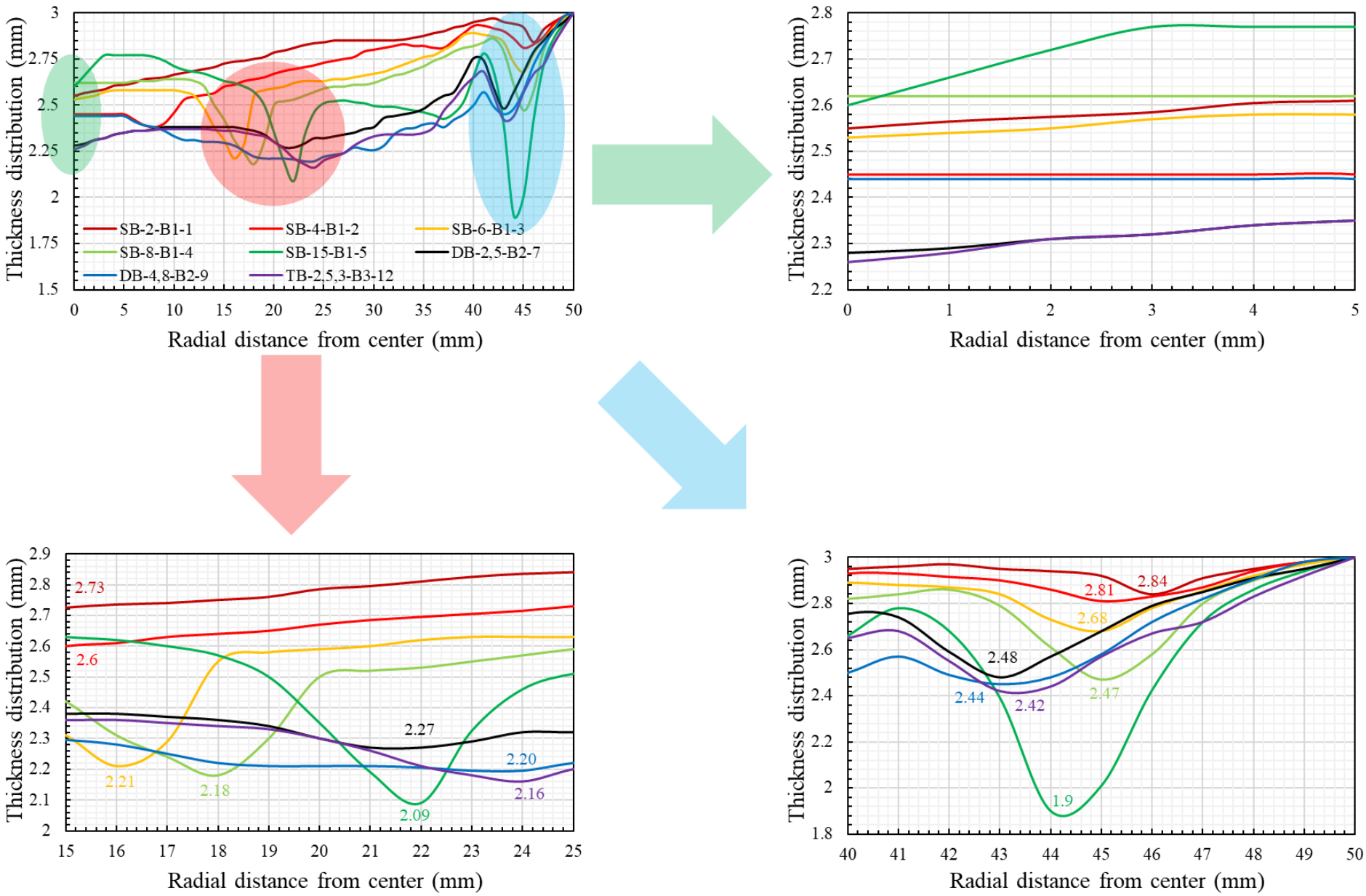


Figure 6. Thickness distribution of the test specimens along the radial distance from the center.

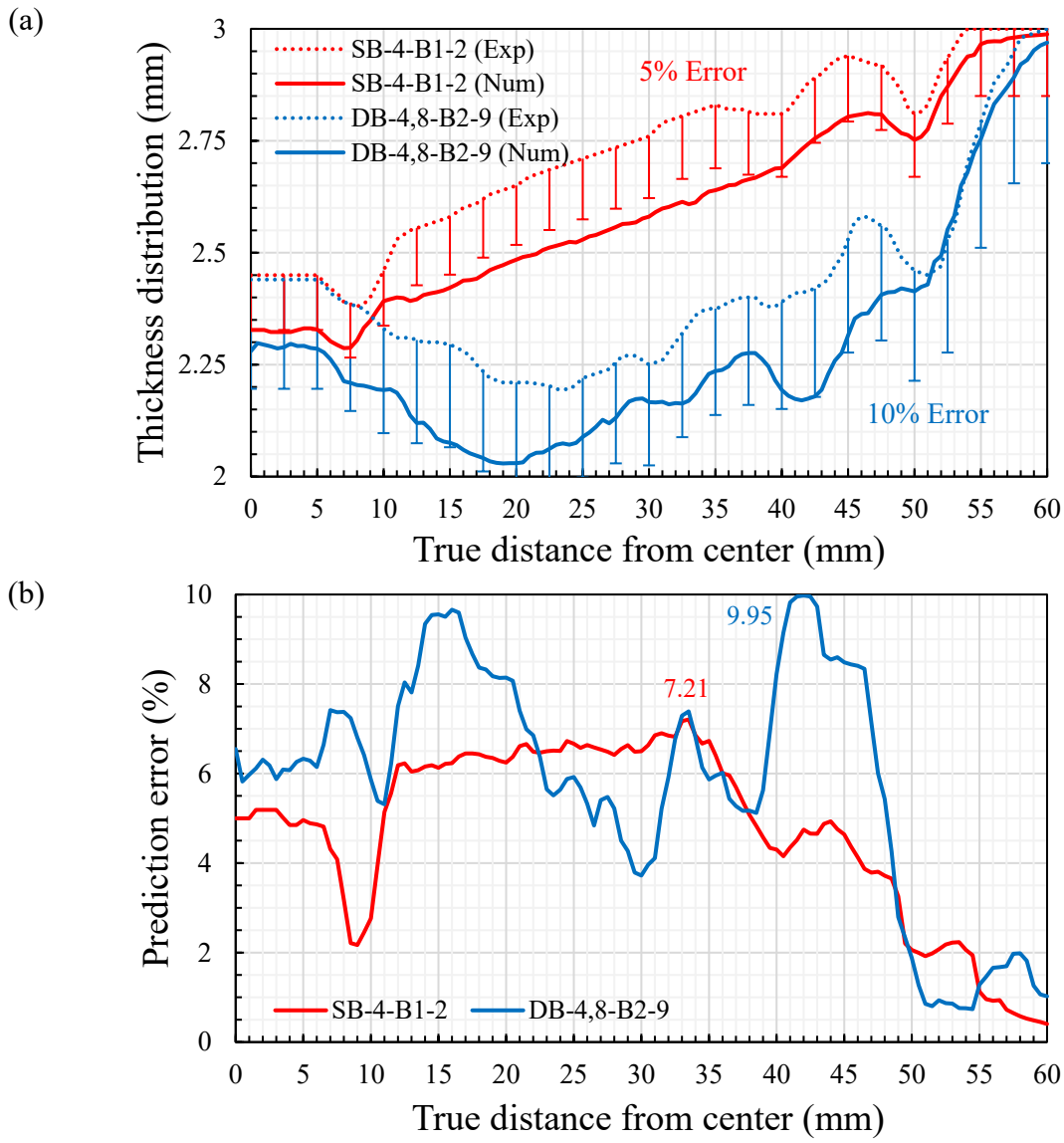


Figure 7. Numerical simulation results versus experiments along the true distance from the center: a) thickness distribution; b) prediction error.

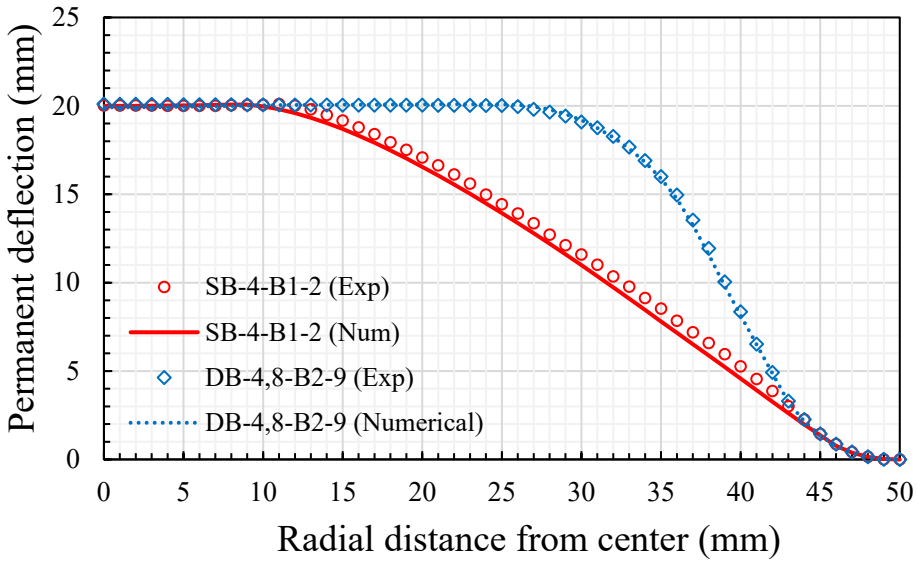


Figure 8. Numerical simulation results versus experiments in terms of the deformation shape profile.

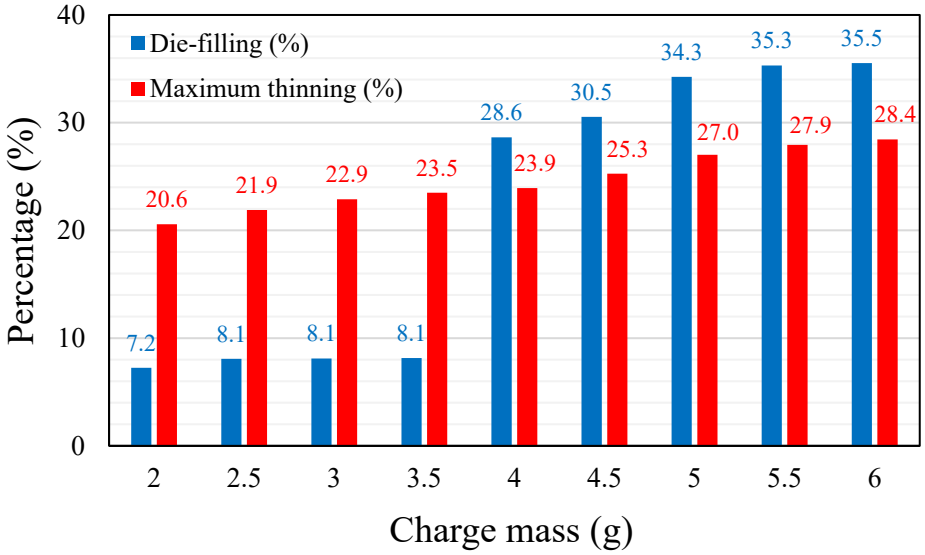


Figure 9. Variations of die filling and thinning in the die–forming by the single underwater explosion process.

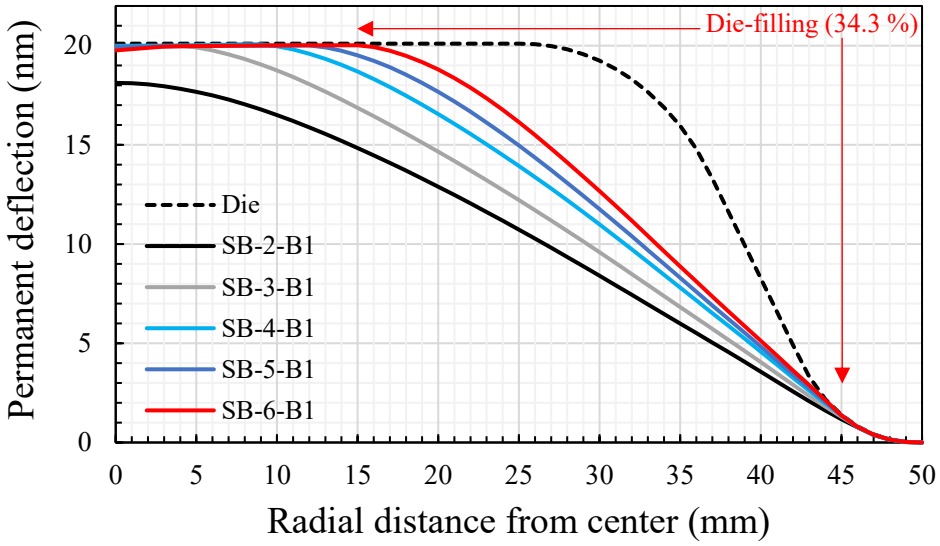
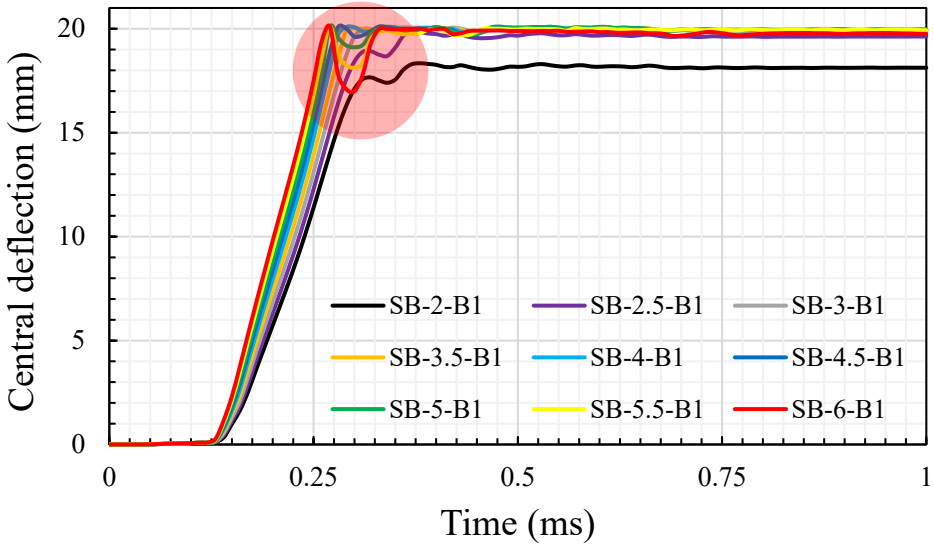


Figure 10. Variations of deformation shape profile for different cases in the die–forming by the single underwater explosion process.

(a)



(b)

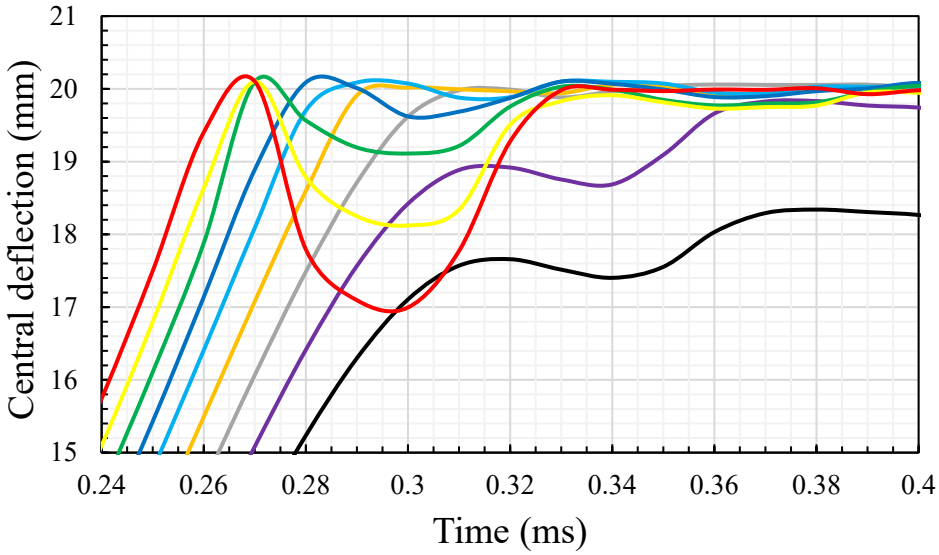


Figure 11. Variations of central permanent deflection in the die–forming by the single underwater explosion process: a) whole process; b) enlarged view.

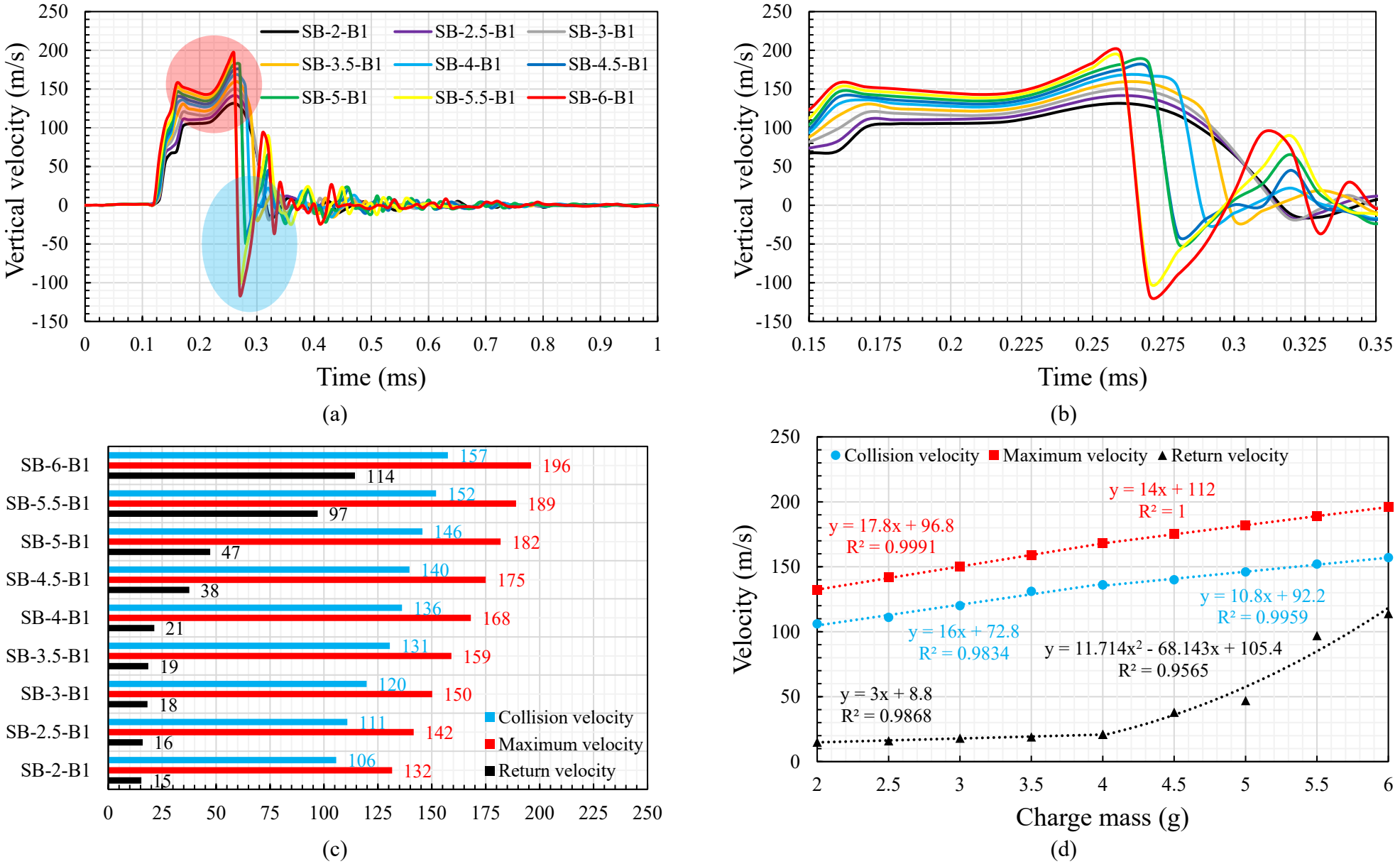


Figure 12. Variations of vertical deformation velocity in the die–forming by the single underwater explosion process: a) whole process; b) enlarged view; c) statistical analysis; d) versus charge mass.

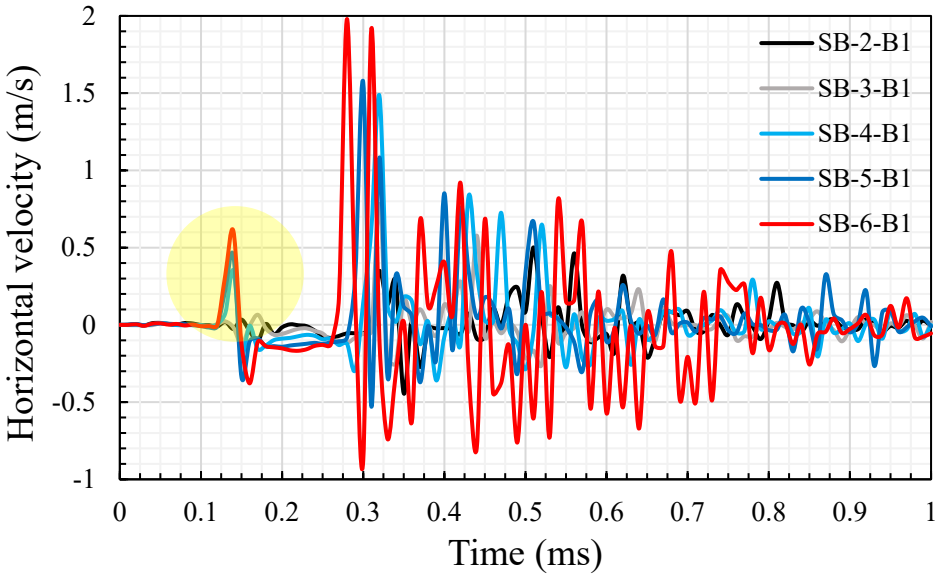
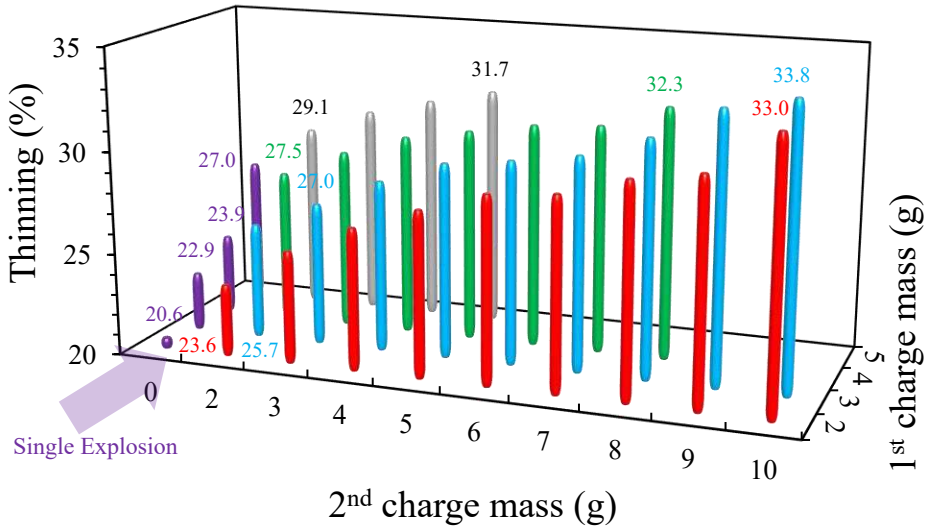
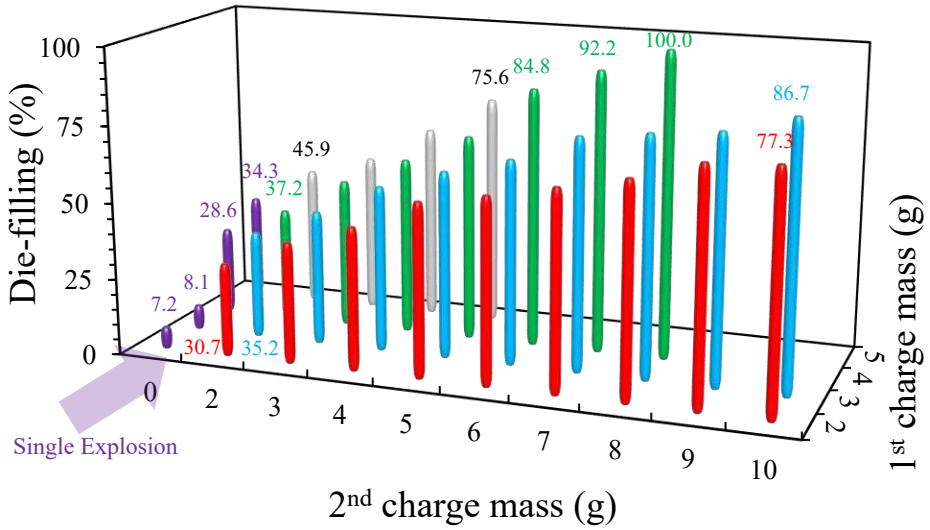


Figure 13. Variations of horizontal deformation velocity in the die–forming by the single underwater explosion process.

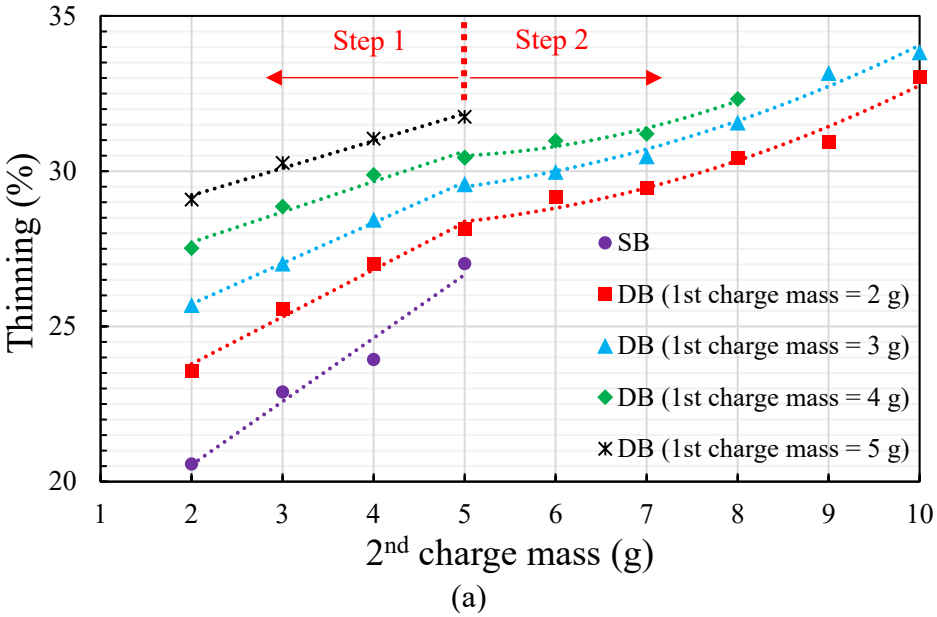


(a)

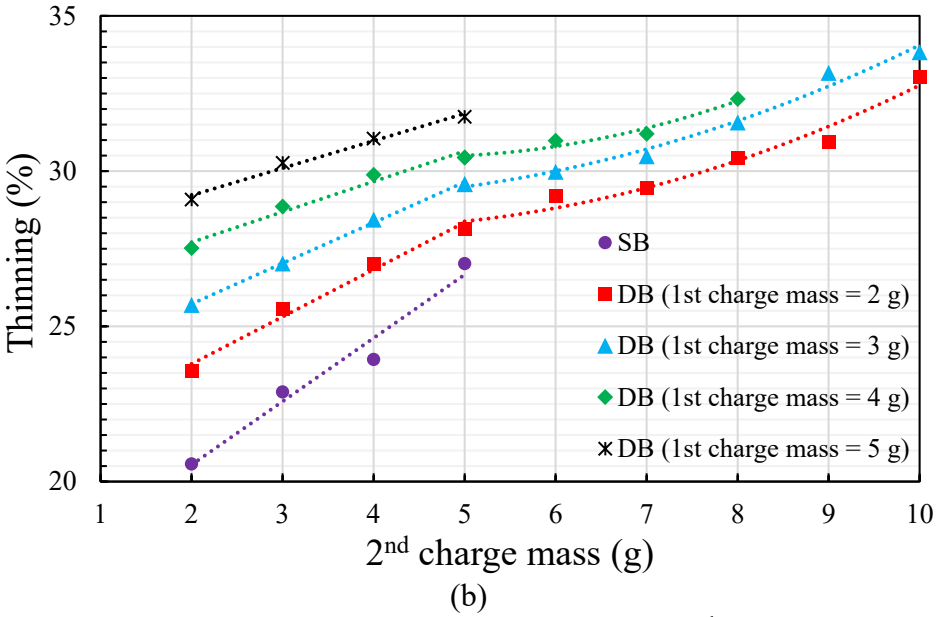


(b)

Figure 14. Variations of die filling and thinning in the die–forming by the double underwater explosion process: a) thinning; b) die–filling.

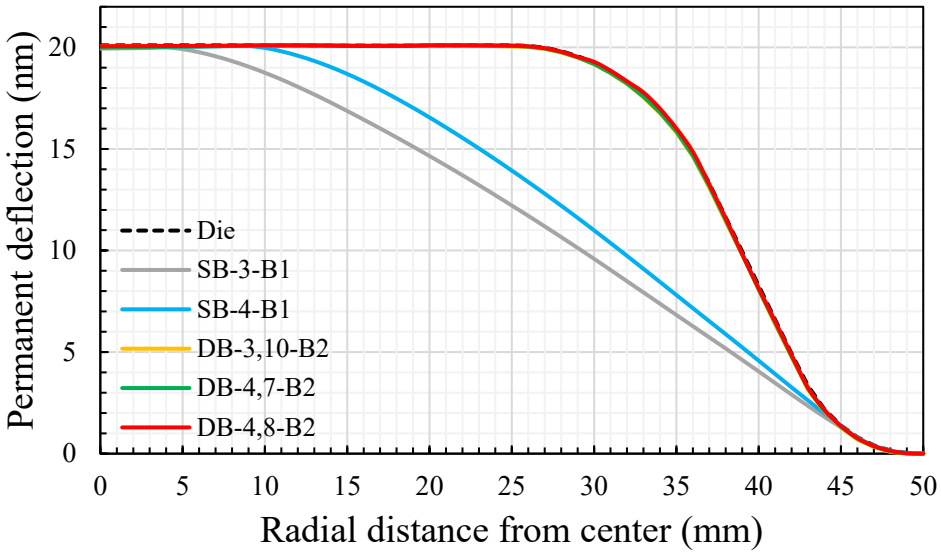


(a)

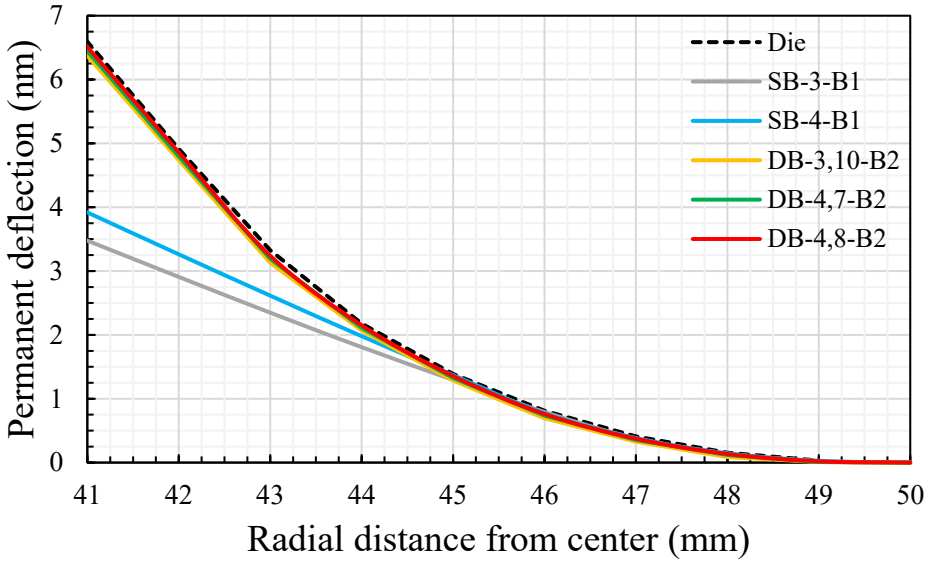


(b)

Figure 15. Variations of die filling and thinning versus the 2nd charge mass in the die–forming by the double underwater explosion process: a) thinning; b) die–filling.

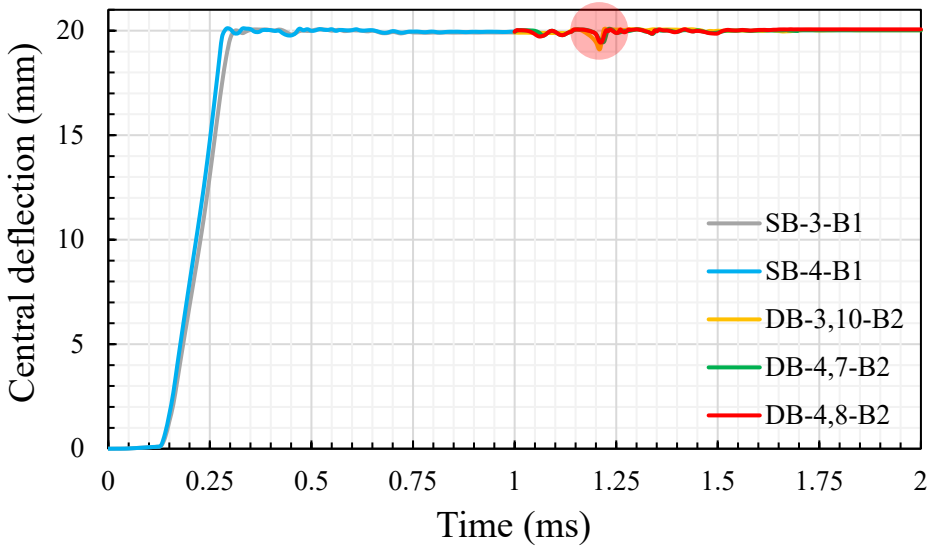


(a)

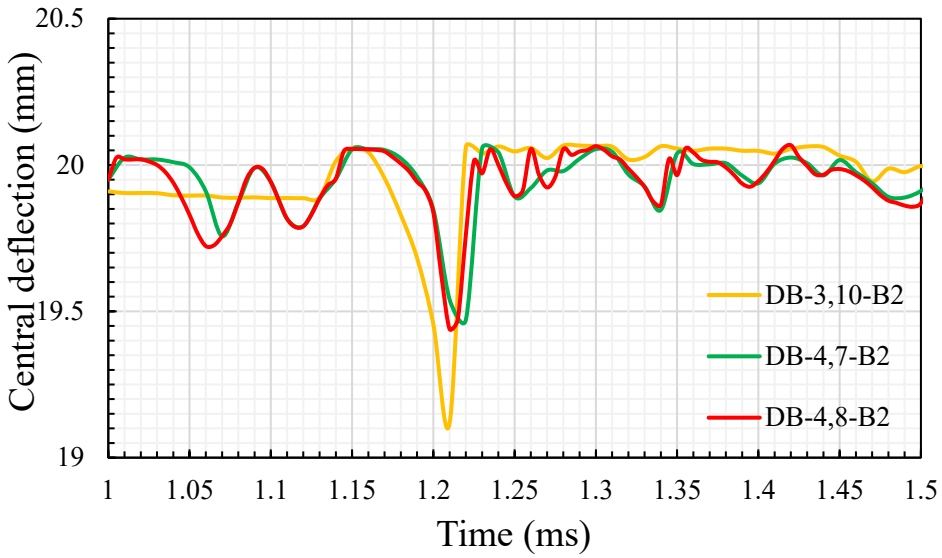


(b)

Figure 16. Variations of deformation shape profile for different cases in the die–forming by the double underwater explosion process: a) overview; b) enlarged view.



(a)



(b)

Figure 17. Variations of central permanent deflection in the die–forming by the double underwater explosion process: a) whole process; b) enlarged view.

20

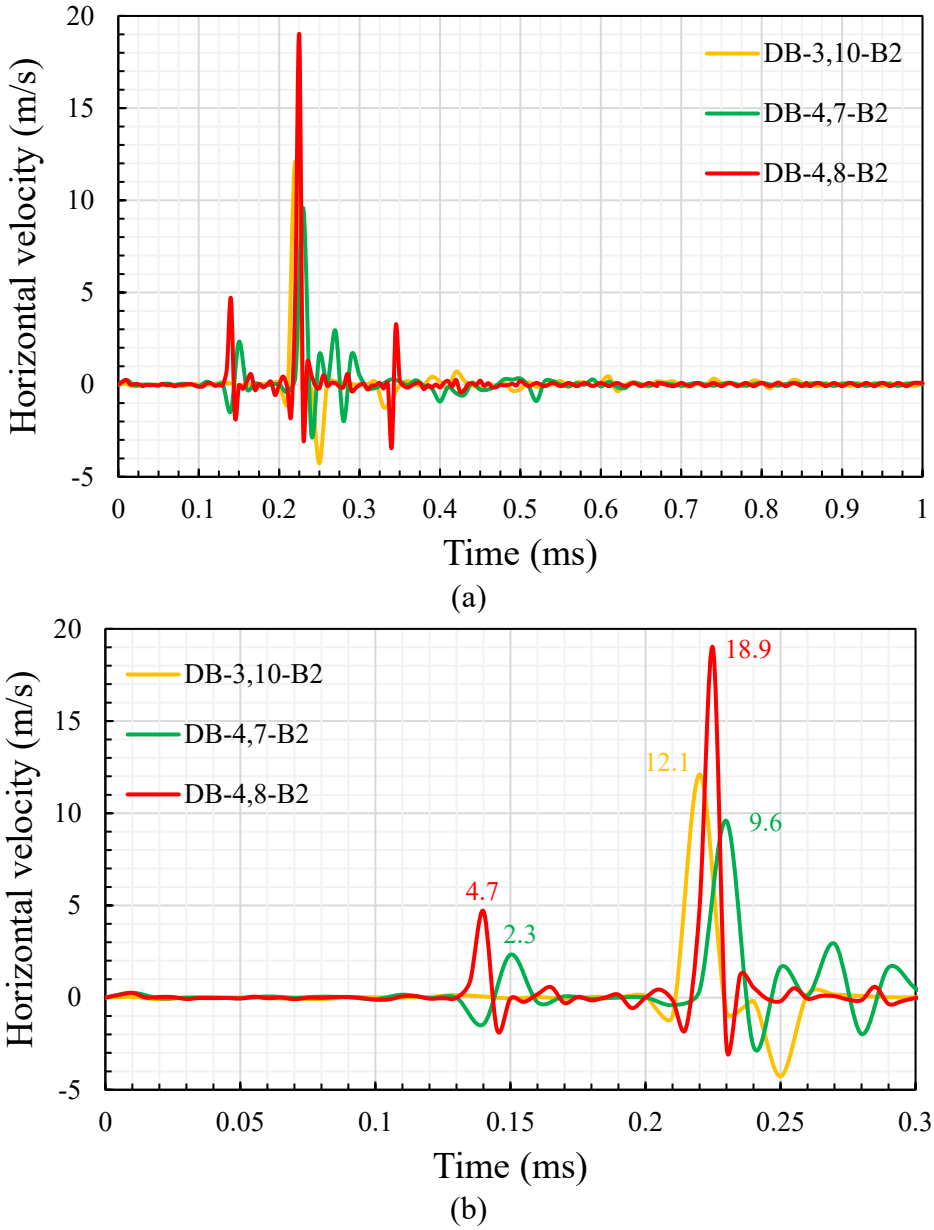


Figure 18. Variations of horizontal deformation velocity in the die–forming by the double underwater explosion process: a) whole process; b) enlarged view.

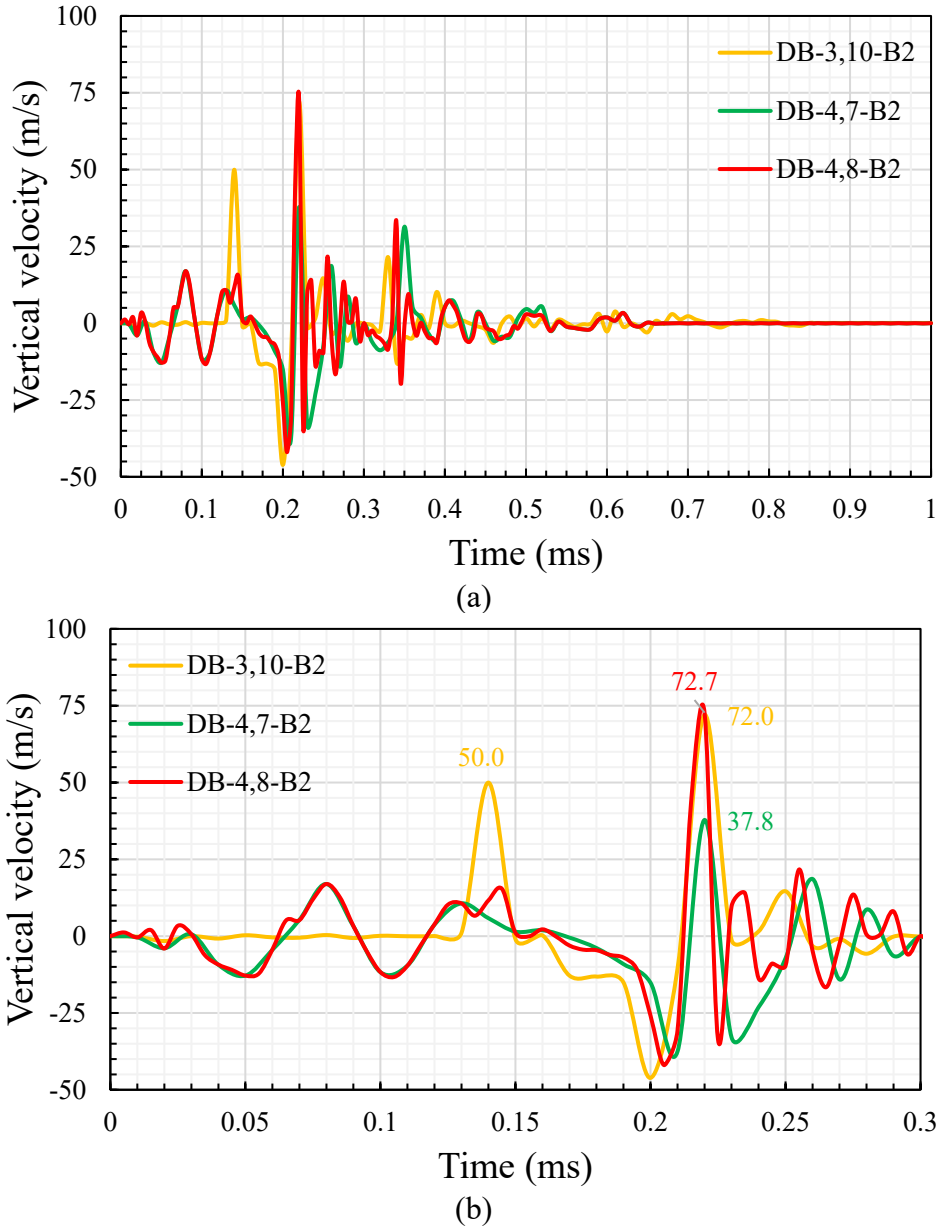
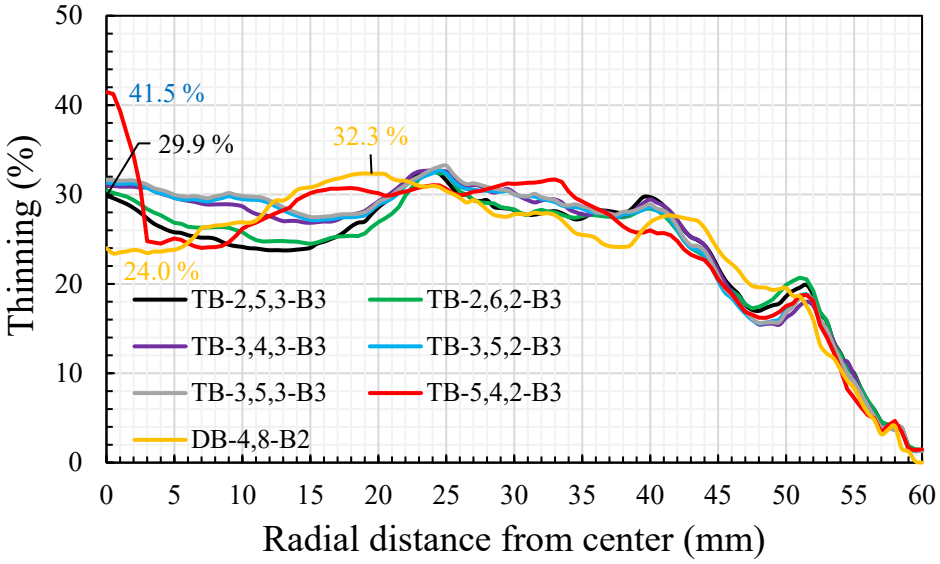
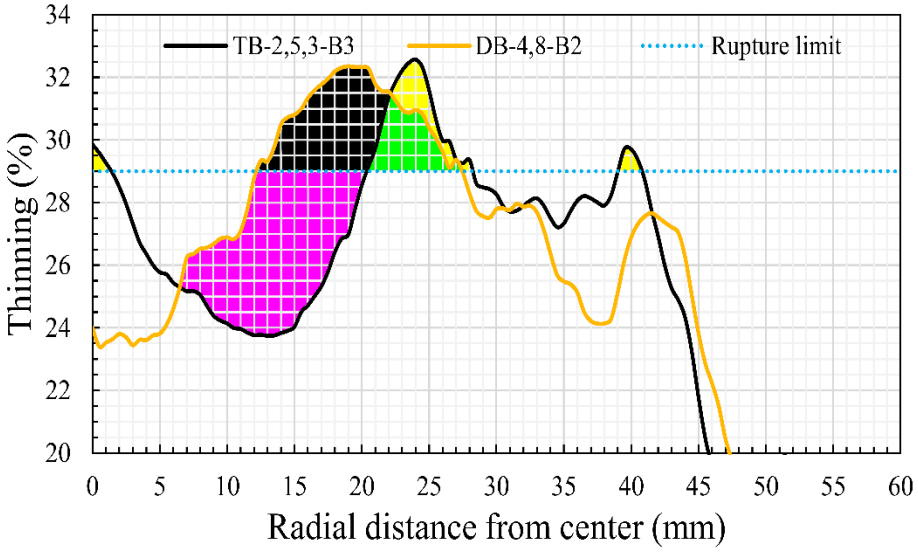


Figure 19. Variations of vertical deformation velocity in the die–forming by the double underwater explosion process: a) whole process; b) enlarged view.

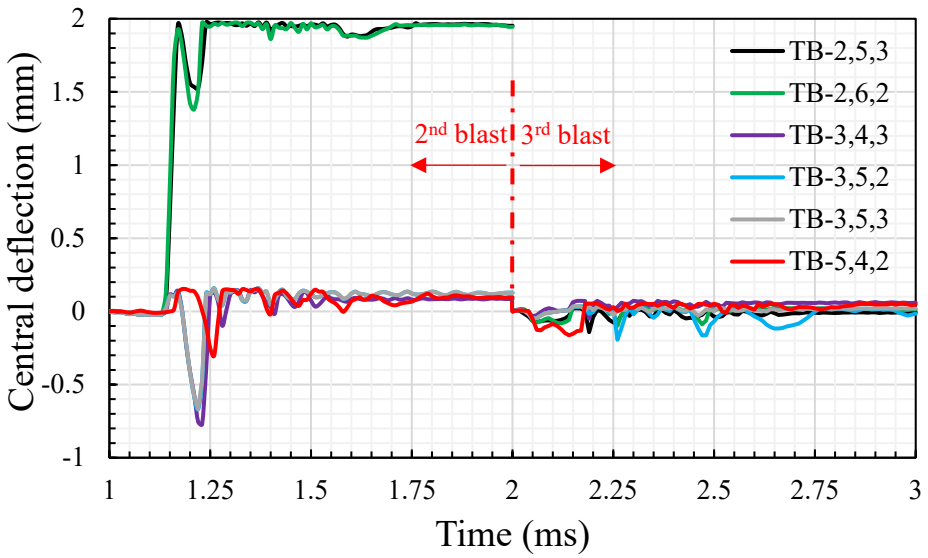


(a)



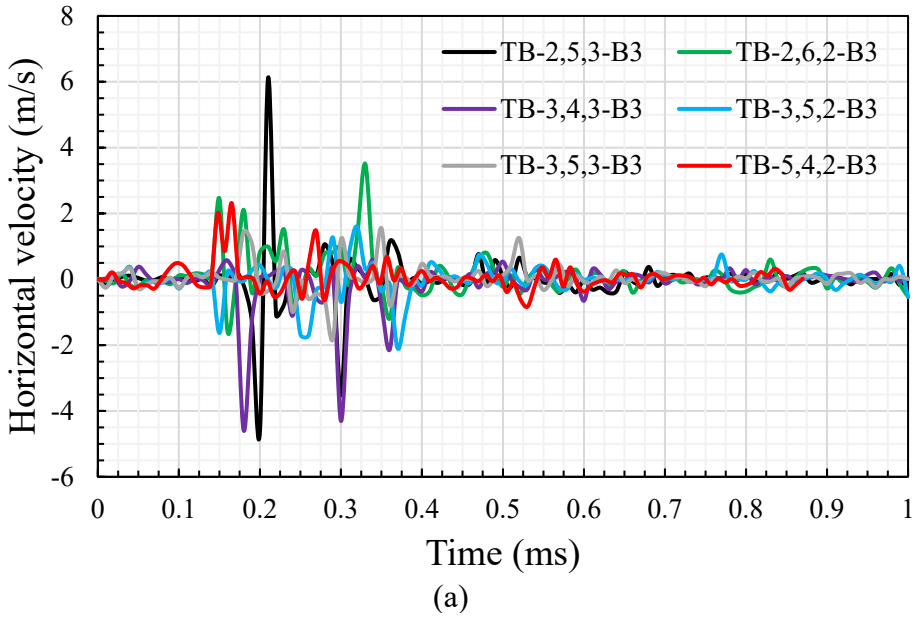
(b)

Figure 20. Variations of thinning in the die–forming by the repeated underwater explosion process: a) different cases; b) enlarged view for two selected cases.

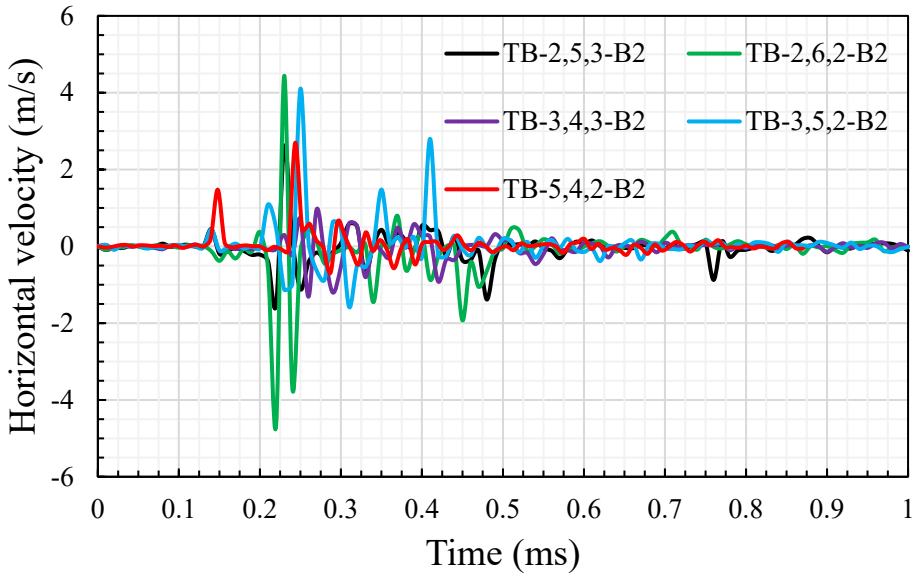


30

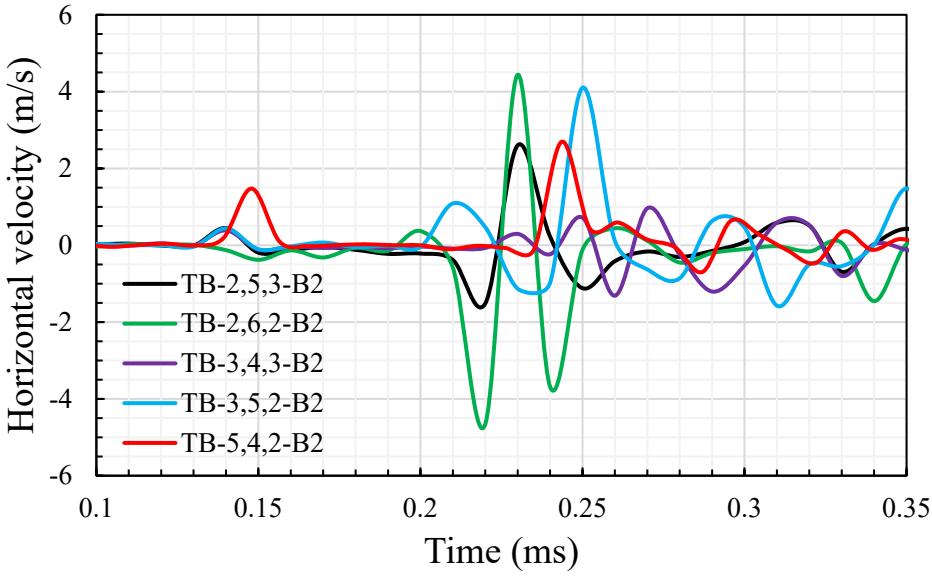
Figure 21. Variations of central permanent deflection in the die–forming by the triple underwater explosion process.



(a)

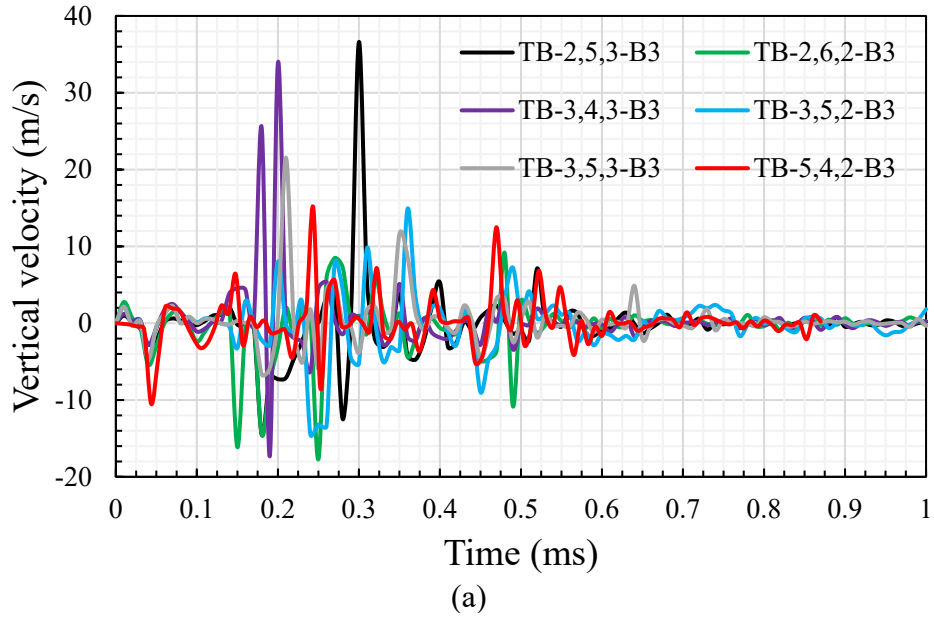


(b)

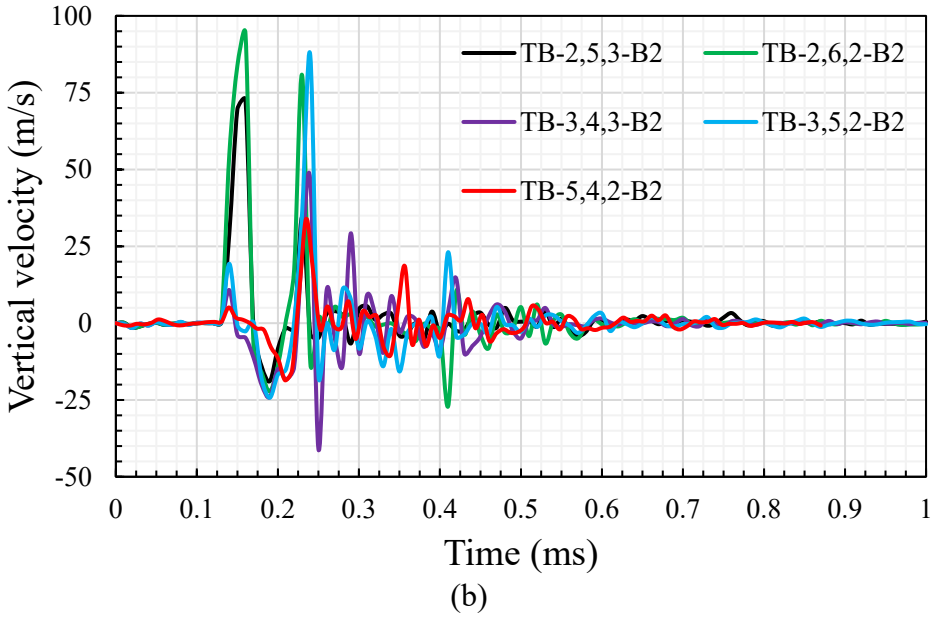


(c)

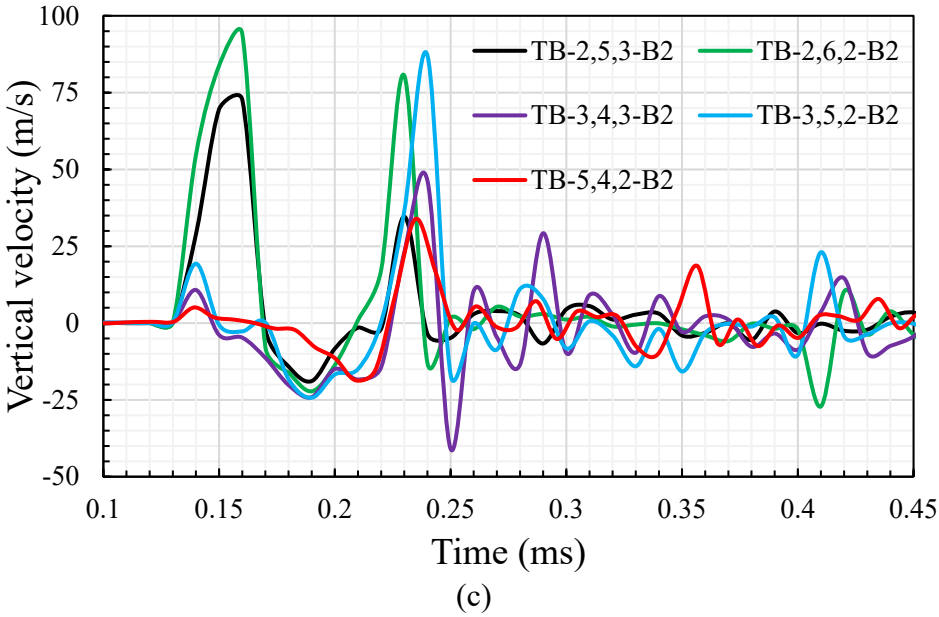
Figure 22. Variations of horizontal deformation velocity in the die–forming by the triple underwater explosion process: a) 3rd blast; b) 2nd blast; c) enlarged view of the 2nd blast.



(a)



(b)



(c)

Figure 23. Variations of vertical deformation velocity in the die–forming by the triple underwater explosion process: a) 3rd blast; b) 2nd blast; c) enlarged view of the 2nd blast.

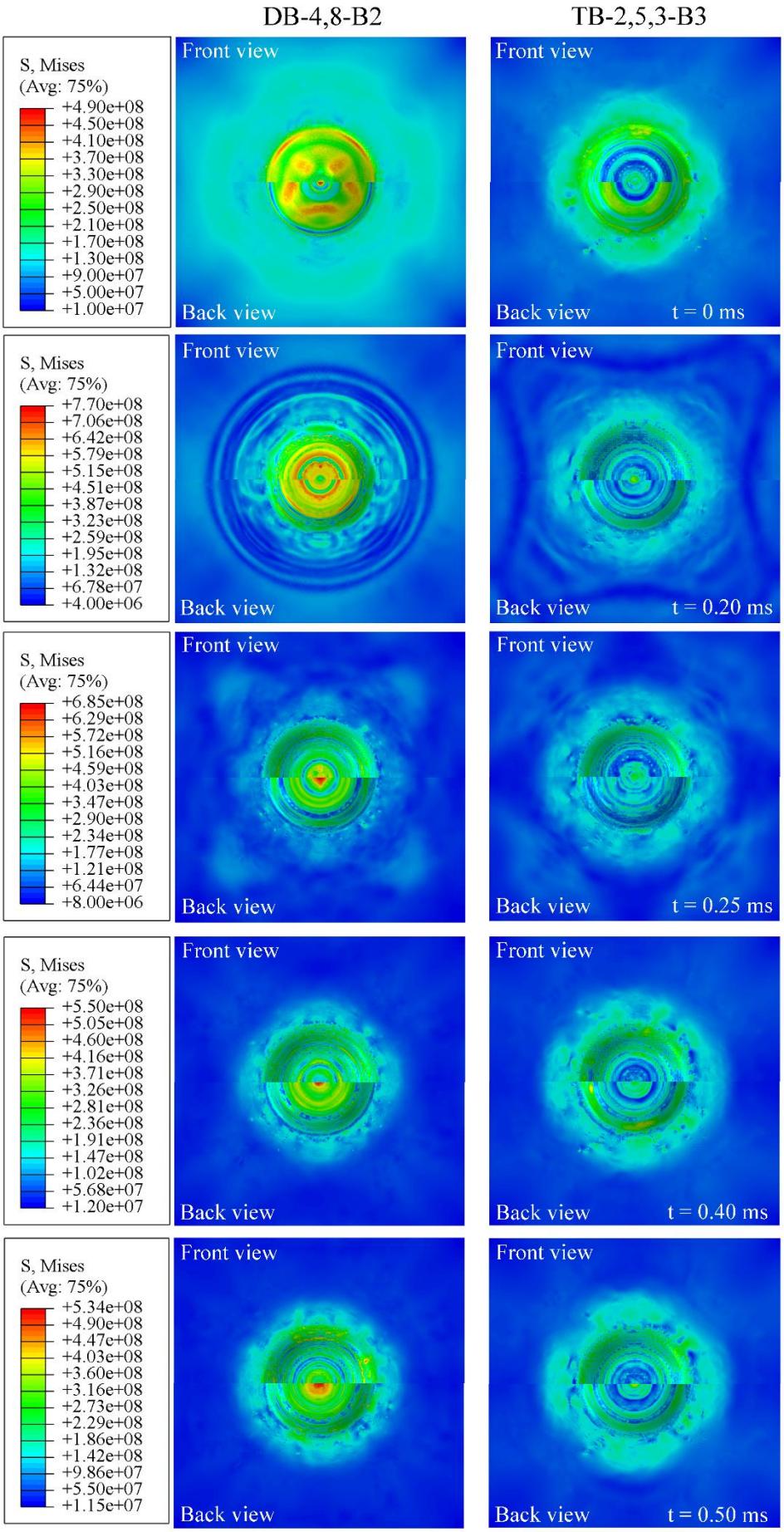


Figure 24. Von Mises stress contour diagram at the last loading cycle obtained by numerical simulation in the die–forming by the repeated underwater explosion process.

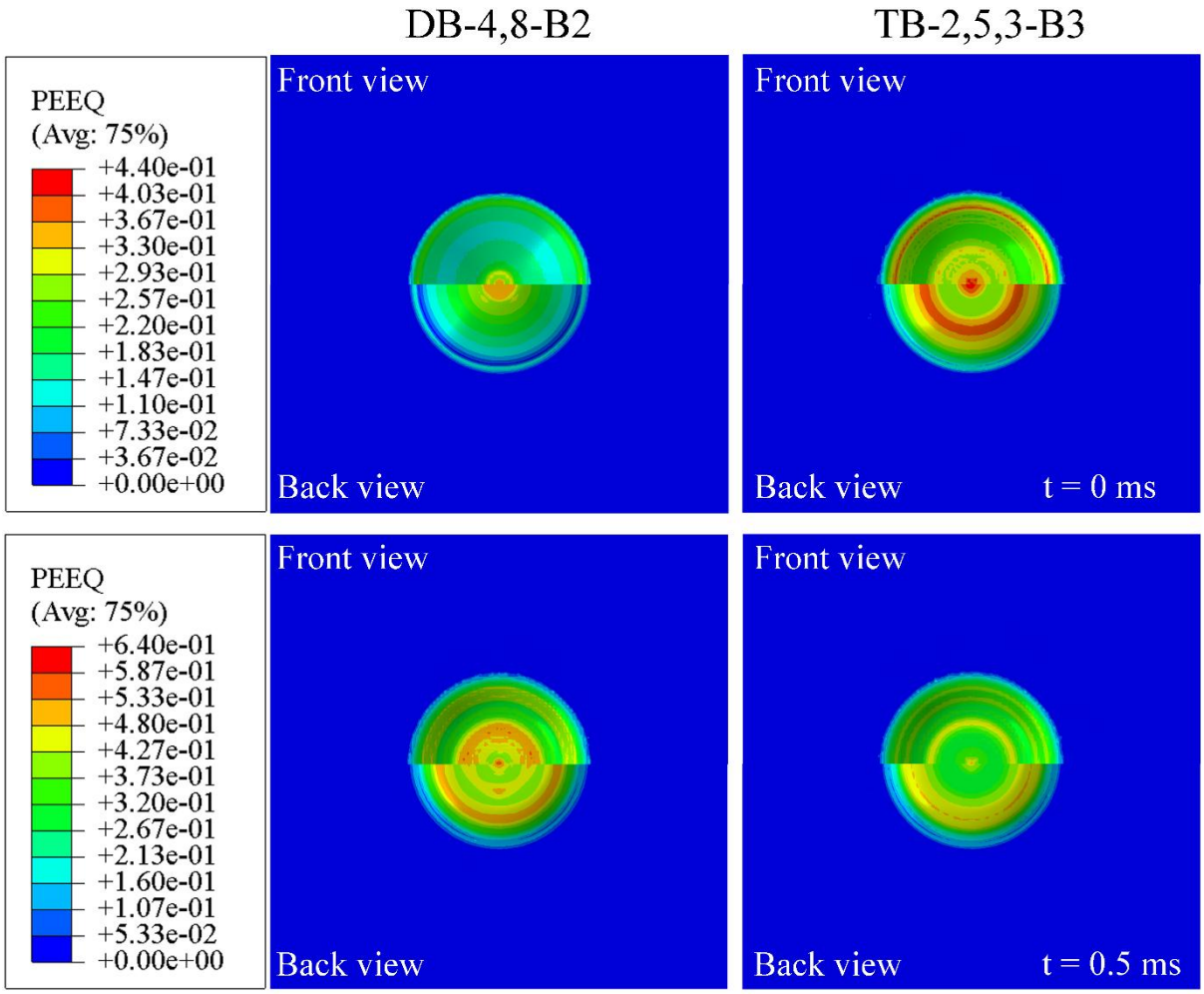


Figure 25. PEEQ contour diagram at the last loading cycle obtained by numerical simulation in the die–forming by the repeated underwater explosion process.

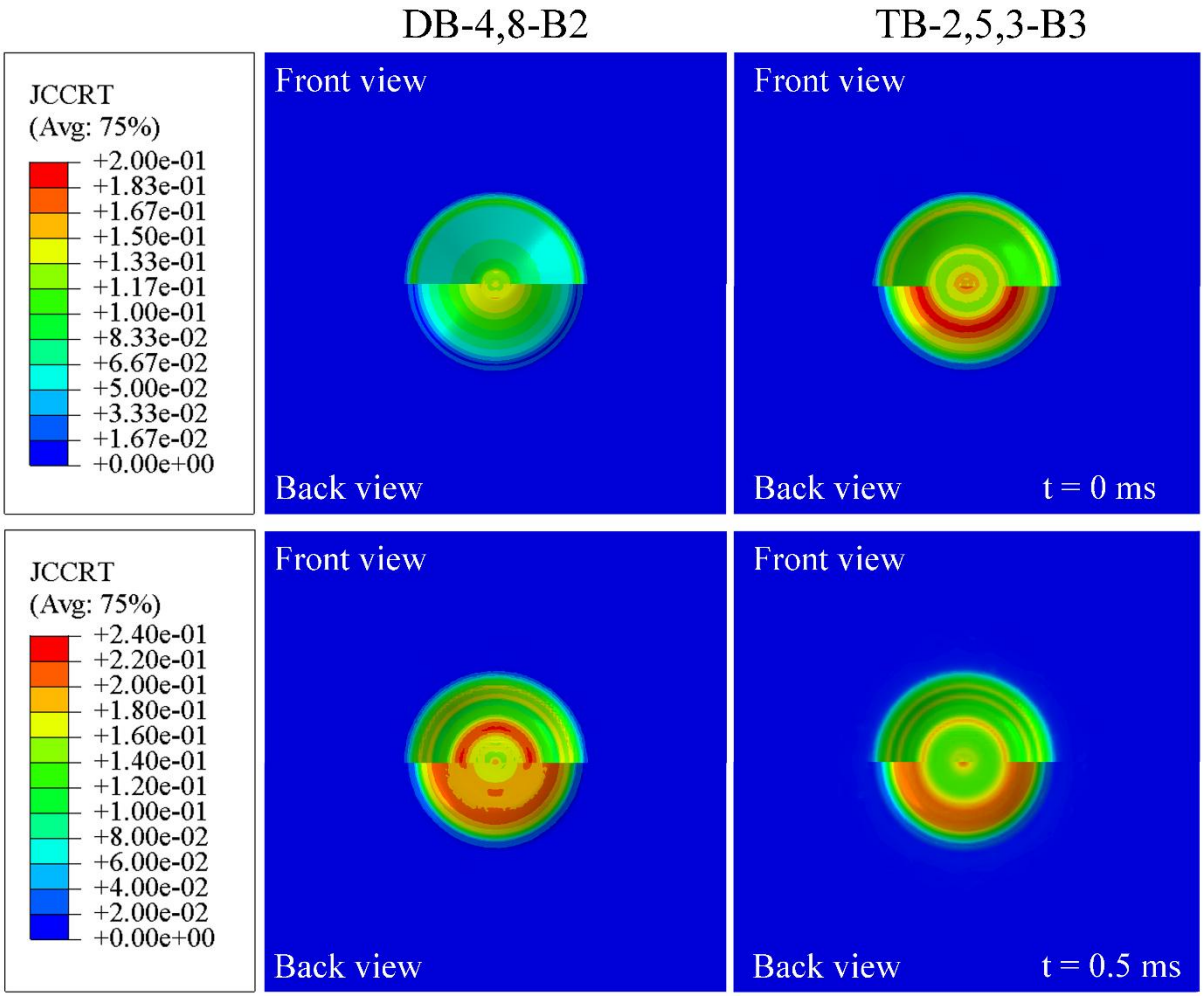


Figure 26. JCCRT contour diagram at the last loading cycle obtained by numerical simulation in the die–forming by the repeated underwater explosion process.